Nucleic Acids Research, 2024, **52**, 7012–7030
https://doi.org/10.1093/nar/gkae453
Advance access publication date: 4 June 2024
Genome integrity, repair and replication

Concurrent D-loop cleavage by Mus81 and Yen1 yields half-crossover precursors

Raquel Carreira [1], Tomas Lama-Diaz[1,†], Maria Crugeiras[1,†], F. Javier Aguado[1,†], Marek Sebesta [2], Lumir Krejci [2,*] and Miguel G. Blanco [1,*]

[1]Department of Biochemistry and Molecular Biology, CIMUS, Universidade de Santiago de Compostela-Instituto de Investigación Sanitaria (IDIS), Santiago de Compostela, A Coruña 15782, Spain
[2]Department of Biology and National Centre for Biomolecular Research, Masaryk University, Brno 62500, Czech Republic

[*]To whom correspondence should be addressed. Tel: +34 881815405; Fax: +34 881815403. Email: miguel.gonzalez.blanco@usc.es
Correspondence may also be addressed to Lumir Krejci. Tel: +420 549493767; Fax: +420 549492556. Email: lkrejci@chemi.muni.cz
[†]The second, third and fourth authors should be regarded as equally contributing Authors.
Present address: Marek Sebesta, CEITEC-Central European Institute of Technology, Masaryk University, Brno 62500, Czech Republic.

Abstract

Homologous recombination involves the formation of branched DNA molecules that may interfere with chromosome segregation. To resolve these persistent joint molecules, cells rely on the activation of structure-selective endonucleases (SSEs) during the late stages of the cell cycle. However, the premature activation of SSEs compromises genome integrity, due to untimely processing of replication and/or recombination intermediates. Here, we used a biochemical approach to show that the budding yeast SSEs Mus81 and Yen1 possess the ability to cleave the central recombination intermediate known as the displacement loop or D-loop. Moreover, we demonstrate that, consistently with previous genetic data, the simultaneous action of Mus81 and Yen1, followed by ligation, is sufficient to recreate the formation of a half-crossover precursor *in vitro*. Our results provide not only mechanistic explanation for the formation of a half-crossover, but also highlight the critical importance for precise regulation of these SSEs to prevent chromosomal rearrangements.

Graphical abstract

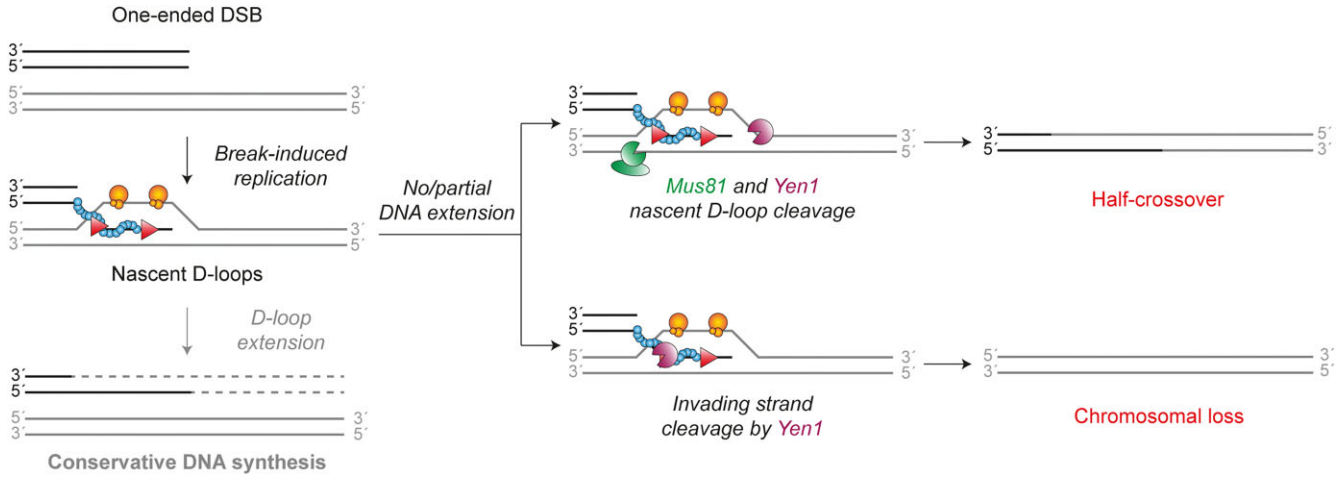

Introduction

Homologous recombination (HR) is an evolutionary-conserved pathway for the repair of DNA double-stranded breaks (DSB), interstrand crosslinks, and protection and processing of stalled replication forks. It relies on the presence of a homologous sequence as a repair template, primarily during the S and G2 phases of the cell cycle when the sister chromatid is available. However, HR occurring between non-allelic regions or homologous chromosomes may result in detrimental outcomes such as loss of heterozygosity (LOH), translocations, or gross chromosomal rearrangements, which have been implicated in human diseases (1,2).

DSB repair through HR involves several sub-pathways, including synthesis-dependent strand annealing (SDSA), double-strand break repair (DSBR), and break-induced replication (BIR). These pathways involve initial resection of the DNA ends to generate 3′-single-stranded DNA (ssDNA) tails (3). These ssDNA tails are rapidly bound by replication protein

Received: September 22, 2023. **Revised:** May 5, 2024. **Editorial Decision:** May 11, 2024. **Accepted:** May 14, 2024

A (RPA), a ssDNA-binding protein, which is subsequently replaced by Rad51 recombinase and facilitated by Rad52 and Rad51 paralogs in budding yeast (4). The resulting Rad51-ssDNA nucleofilament enables homology search and DNA strand invasion into a donor template. This invasion event creates a joint molecule known as a displacement-loop (D-loop), which represents the central intermediate in HR repair (2,5–7). In yeast, Rad54 is required for D-loop formation and consequent Rad51 displacement from the heteroduplex DNA (8–11), enabling DNA polymerase (Pol) δ access to the invading 3′-end (12). To prevent the formation of undesirable crossovers (COs), extended D-loops can be disrupted by helicases such as Sgs1-Top3-Rmi1 (STR) (13), Srs2 (14,15) or Mph1 (16,17). The extended, displaced strand anneals with the second end of the original DSB within SDSA pathway, leading exclusively to non-crossovers (NCO). Alternatively, if the displaced strand of the extended D-loop reanneals with the second end of the initial DSB, it may lead to the formation of a double Holliday junction (dHJ) (18), the characteristic intermediate of the DSBR model. The dHJ can be either dissolved by the STR complex, generating exclusively NCOs (19,20) or cleaved by structure selective-endonucleases (SSEs), such as Slx1-Slx4, Mus81-Mms4 (Mus81), and/or Yen1, generating both NCOs and COs (21,22).

However, when only one end is available for annealing, as in single-ended DSBs at collapsed replication forks or eroded telomeres, the repair proceeds through BIR (23). This pathway involves bubble-migration-driven DNA synthesis via D-loop branch migration, leading to the conservative inheritance of newly synthesized DNA (24–26). This may lead to unrestrained, highly mutagenic DNA synthesis extending to the end of the chromosome unless restricted by a converging fork or D-loop disruption by Mus81 (27). Asynchrony between leading and lagging strand synthesis leads to the accumulation of ssDNA, increasing the risk of mutagenesis (28–30). When occurring between homologous chromosomes, BIR may also derive in extensive LOH or non-reciprocal translocations (31,32). Moreover, multiple rounds of strand invasion during BIR may drive complex genome rearrangements if happening within disperse repeat sequences (33–35). Premature resolution of BIR intermediates might also result in half-crossover (HC) events (36,37), which involves fusion between recipient and donor molecules and generation of a new, one-ended DSB on the donor chromosome, potentially resulting in additional rounds of HC formation known as half-crossover cascades (HCCs) (29,38).

Mus81 and Yen1 have been implicated in the generation of complex chromosomal rearrangements during BIR, including HC events and translocations, by cleaving the D-loop intermediate (35). Previous studies suggested that HC formation in the absence of a fully functional Polδ complex is partially Mus81-dependent (37), and that premature activation of Yen1 can hinder BIR progression and lead to an increase in chromosomal loss (CL) and HC events (28). Moreover, these SSEs have recently been implicated in the generation of multi-invasion mediated-rearrangements (MIR), a novel source of genetic instability mechanistically similar to HCCs (39–42). Ample biochemical evidence exists regarding how the Mus81 complexes from multiple organisms recognize and cleave a variety of branched DNA substrates, including synthetic oligonucleotide-based D-loop substrates (43–45). Specifically, Mus81-Mms4 from budding yeast operates as a single heterodimer that can process branched DNA substrates containing a nick at the junction point. Upon binding, both the enzyme and the substrate undergo conformational changes that position the catalytic residues typically 4 nucleotides upstream the 5′ end of the branch point, guiding the cleavage process (46–49). Contrarily, little is known about Yen1's ability to process such synthetic structures. Moreover, it remains unclear if these SSEs can process more physiologically relevant Rad51-mediated D-loops, where the proteins involved in D-loop formation could modulate or interfere with their activity, as evidenced in related biochemical experiments (13,14,30,50–52).

In this study, we used a biochemical approach to investigate the processing capabilities of Mus81 and Yen1 on various oligonucleotide-based or Rad51-mediated D-loop structures. Our data demonstrate that Yen1 can effectively process all tested D-loop substrates. In contrast, Mus81 fails to cleave D-loops with a ssDNA-overhang. Moreover, by mapping the cleavage sites of these nucleases on synthetic and enzymatically reconstituted D-loops, we provide evidence supporting their compatibility with the generation of HC and CL events. Importantly, we observed that the simultaneous actions of Mus81 and Yen1 in plasmid-based assays create a double-nicked D-loop structure that can be ligated to form a direct precursor of a half-crossover product. These biochemical results provide mechanistic explanation for the existing genetic evidence that the combined actions of Yen1 and Mus81 on a D-loop contribute to the generation of complex genome rearrangements in the context of BIR and MIR.

Materials and methods

Recombinant proteins

Yen1 and the catalytically inactive mutant Yen1ND (E193A, E195A) were purified as C-terminally tagged 3xFLAG-2xTEV-10xHIS fusion proteins, as previously described (53). Mus81-Mms4 and the catalytically inactive mutant Mus81-Mms4ND (D414A, D415A) were purified as N-terminally tagged 3xFLAG and 10xHIS-StrepII protein fusions, as described elsewhere (54). DNA-damage sensitivity assays (see below) were carried out to ensure that the tagged versions of the enzymes retain biological activity (Supplementary Figure S1A, B). Rad51, RPA, and Rad54 were purified according to described procedures (55). RecA was obtained from New England Biolabs (#M0249S) and SSB from Thermo Fisher Scientific (#70032Z500G). Protein concentrations were determined using the Bradford assay (Bio-Rad) and densitometry of Coomassie-stained PAGE gels, using bovine serum albumin (BSA) as a standard. All protein batches were tested for exonuclease, endonuclease, and protease contaminant activities, and were analysed by SDS-PAGE followed by Coomassie staining (Figure 1B and Supplementary Figure S4A).

Oligonucleotide purification and annealing into DNA substrates

The oligonucleotides used in this study (Supplementary Table S1) were obtained from Merck, subjected to PAGE purification, and annealed as detailed previously (53). Shortly, labelled, and unlabelled oligonucleotides were mixed at a 1:3 ratio, boiled in a water bath, and cooled down to room temperature overnight. Fully annealed substrates were purified from 10% native PAGE gels in 1× Tris–borate–EDTA

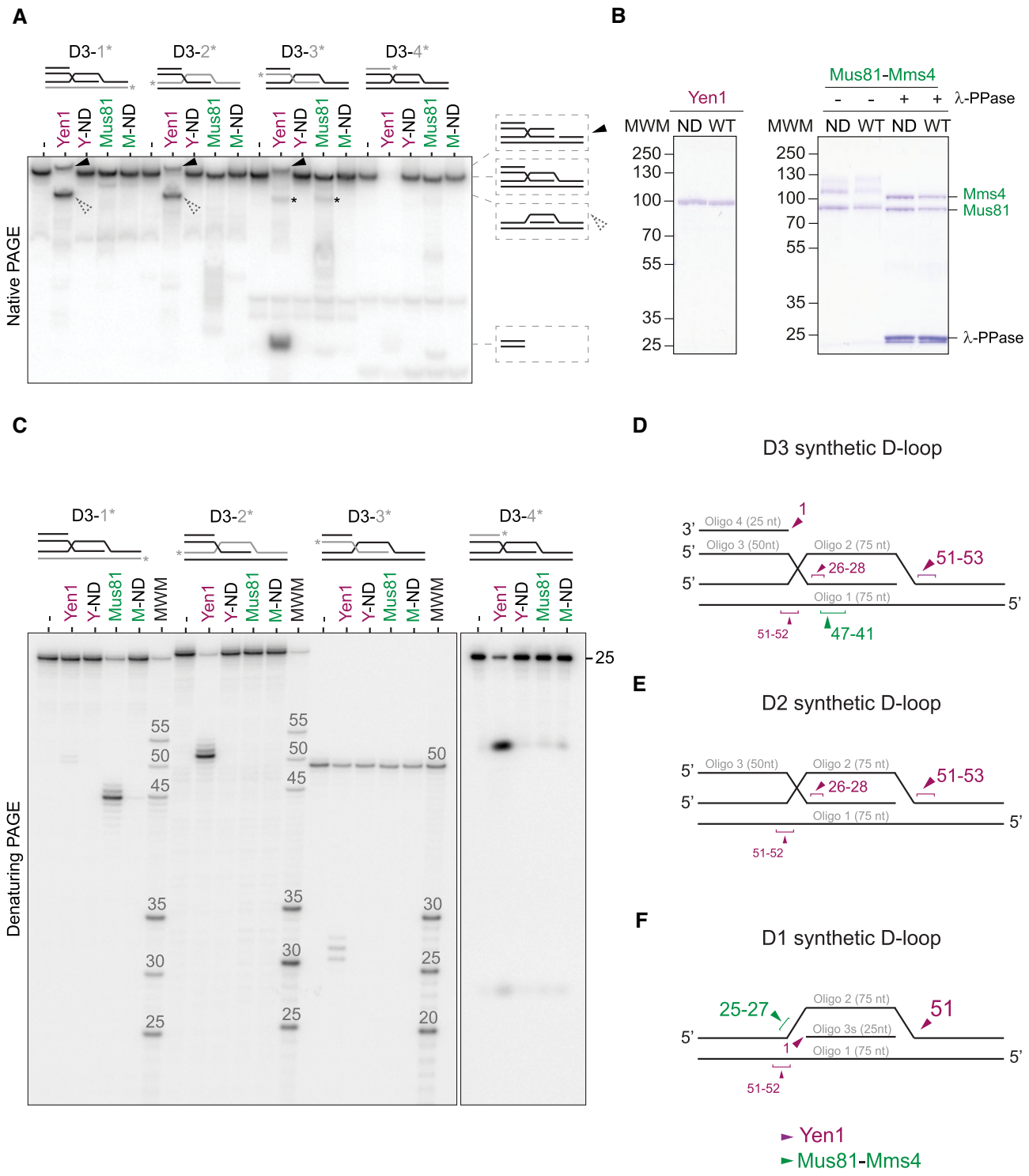

Figure 1. Yen1 and Mus81 cleavage of synthetic D-loops. (**A**) Synthetic D3 D-loops (D3) were ^{32}P-labelled at the 5′-end (asterisk) of the indicated strand (grey) and incubated with 10 nM Yen1^{WT} (Yen1), Yen1ND (Y-ND), Mus81^{WT} (Mus81), or Mus81ND (M-ND) for 10 min at 30°C. (–) indicates no enzyme. The reaction products were analysed using 10% native PAGE and phosphorimaged. Schematic representations of the substrate and cleavage products are shown on the right. Black arrowheads indicate the first product shown on the right, dotted arrowheads indicate the third product shown on the right. Asterisks indicate two bands that are likely to arise from cleavage of oligonucleotide 1, which in itself does not alter electrophoretic migration, followed by partial disassembly of the nicked D-loop. (**B**) Purified Yen1ND, Yen1^{WT}, Mus81-Mms4ND, and Mus8-Mms4^{WT} proteins (with or without a lambda-phosphatase (λ-PPase) treatment), were analysed by SDS-PAGE, and stained with Coomassie. Molecular weight markers are indicated in kDa. (**C**) The same reaction products as in (A) were analysed using 10% denaturing PAGE. A molecular weight marker (MWM) consisting of a mixture of 5′-^{32}P end-labelled oligos of defined length with the same sequence as the labelled oligo was used, therefore MWM bands differ between lanes. D3-4* samples (split panel) were loaded later on the same gel, to allow visualization of small products. (**D**) A schematic representation of Yen1 (purple) and Mus81 (green) incision sites on the oligonucleotide-based D3 D-loop. The arrowhead and number size indicate the relative efficiency of the cleavage. (**E**) same as (D), but for a D2 D-loop structure. (**F**) Same as (D), but for the D1 D-loop structure.

(1× TBE) buffer (90 mM Boric acid, 90 mM Tris-base, 2 mM EDTA). For radioactive substrates, oligonucleotides were 5′-end-labelled with [γ-^{32}P]-ATP (3000 Ci/mmol, Perkin Elmer) and T4 polynucleotide kinase (PNK; Thermo Fisher, #EK0031), according to standard procedures. Fluorescent substrates utilized 5′- and/or 3′-Cy5 or Cy3 labelled oligonucleotides. In the indicated cases, oligonucleotides containing three consecutive phosphorothioate (SP) linkages were used. The unpaired regions of these junctions are composed of heterologous sequences to prevent substrate dissociation by spontaneous branch migration. The strand composition of each substrate is detailed in Supplementary Table S2.

The plasmid DNA (pBluescript SK (–), pBSK, 2958 bp) was purified using commercial DNA purification kits (GenElute™ HP Plasmid Miniprep kit, Merck, #NA0160), according to standard procedures. To minimize plasmid nicking, which could affect the subsequent D-loop formation that requires negatively supercoiled plasmids (8,56), the cell pellet was re-suspended by pipetting and centrifugation steps were carried out at 8000 × *g*.

Endonuclease assays with oligonucleotide-based substrates

For the experiments using radioactively labelled oligonucleotide-based D-loops (Figure 1 and Supplementary Figure S2), 10 nM protein was incubated with ∼1 nM 5′-^{32}P end-labelled substrate in 25 μl of reaction buffer (Yen1 reaction buffer: 50 mM Tris–HCl pH 7.5, 0.5 mM $MgCl_2$; Mus81-Mms4 reaction buffer: 25 mM Tris–HCl pH 7.5, 3 mM $MgCl_2$, 100 mM NaCl, 0.1 mM DTT, 0.1 μg/ml BSA). In all reactions, enzymes represent 1/10 of the final volume (or enzyme storage buffer in mock reactions). After 10 min incubation at 30°C, 10 μl of each reaction was deproteinized by addition of 2 μl STOP solution (1.5% SDS, 10 mg/ml proteinase K (PK)) and incubation at 37°C for 1 h, followed by incorporation of 0.2 vol of 6× Ficoll loading buffer (15% Ficoll-400, 60 mM EDTA, 20 mM Tris–HCl pH 8.0, 0.5% SDS). Another aliquot of 10 μl was mixed with 1 vol of 2× denaturing loading buffer (1× TBE, 80% formamide) and incubated at 99°C for 3 min. The radiolabelled products were then separated by PAGE through 10% native or denaturing (7 M urea) PAGE gels in 1× TBE buffer. After electrophoresis, gels were dried onto 3MM Whatman chromatography paper (GE Healthcare), exposed to a phosphor screen (Fujifilm), visualized in a Typhoon FLA9500 (GE Healthcare), and quantified by densitometry using ImageQuant software (GE Healthcare).

For kinetics experiments using fluorescently labelled oligonucleotide-based D-loops (D3, D3-SP, and nicked D3) (Figure 2), 20 nM protein was incubated with 10 nM 5′-Cy5 and 5′-Cy3 labelled substrate. Reactions were performed as described above. Aliquots were withdrawn at the indicated times (0, 0.5, 1, 2, 4, 8, 16, 32, 64, 128 min) and analysed by 10% native and denaturing (7 M urea) PAGE in 1× TBE buffer. Fresh gels were scanned in a Typhoon FLA9500 and quantified by densitometry using ImageQuant software. Each experiment was done in triplicate.

For experiments using the long 3′-flap substrate, 2 μl of the indicated final concentration of RPA (25, 50, 100, 200, 400, and 600 nM) was pre-incubated with 40 nM 5′-Cy5-labelled 3′-flap for 10 min at 37°C in 8 μl Mus81-D-loop buffer (see next section). Then, 1 μl of Mus81-Mms4 at 400 nM final concentration was added and incubated for another 10 min at 30°C. Reactions were deproteinized by the addition of 2 μl STOP solution (1.5% SDS, 10 mg/ml PK) and incubation at 37°C for 1 h, followed by incorporation of 0.2 vol 6× Ficoll loading buffer. Reaction products were analysed through 10% native PAGE in 1× TBE buffer. Fresh gels were scanned in a Typhoon FLA9500 and quantified by densitometry using ImageQuant software.

Endonuclease assays with plasmid-based D-loops

Rad51/Rad54-mediated D-loops

To form the different D-loop structures, 40 nM of the indicated fluorescently labelled DNA molecule (this equals to 3.6, 4.0, and 4.8 μM nucleotides for D1, D2, and D3, respectively) was incubated with 2 μM Rad51 in D-loop buffer (35 mM Tris–HCl pH 7.5, 50 mM KCl, 1 mM DTT, 2 mM ATP, 20 mM creatine phosphate, 20 μg/ml creatine kinase), and 2.5 mM $MgCl_2$ for Mus81-Mms4 reactions or 1.5 mM $MgCl_2$ for Yen1 reactions) for 5 min at 37°C. When appropriate, RPA or SSB (600 nM) were added to the nucleoprotein filament and incubated for another 4 min, followed by the addition of Rad54 (300 nM) and incubation at 23°C for 3 min. D-loop formation was initiated by the addition of 2 μl pBSK (1/5 total volume, 64 ng/μl, 35 nM in molecules, 200 μM in nucleotides) in 10 μl final reaction volume and incubated for 5 min at 23°C. Under these conditions, the molar ratio between Rad51 and the invading oligos is 50, which equals to a 0.55 (D1), 0.50 (D2), and 0.625 (D3) Rad51: ssDNA nt ratio (90 nt ssDNA in D1; 100 nt ssDNA in D2; 80 nt ssDNA in D3). For RPA/SSB, its molar ratio with respect to the invading oligos is 15, which equals to a 0.16 (D1), 0.15 (D2), and 0.18 (D3) RPA: ssDNA nt ratio. The Rad54/pBSK donor plasmid ratio is 8.5. After D-loop formation, 1 μl at the indicated concentration of Yen1, Mus81-Mms4, the nuclease-dead mutants (always at the highest concentration used for the catalytically active enzyme), or storage buffer were added to the reaction, followed by incubation at 30°C for the indicated times. Reactions were then deproteinized by the addition of 1.5 μl STOP solution (0.9 % SDS, 1mg/ml PK) and incubated at 37°C for 10 min, followed by the addition of 0.2 vol 6× glycerol loading buffer (66% Glycerol, 66 mM EDTA, 11 mM Tris–HCl pH 7.5). Reactions were analysed by electrophoresis in a 0.9% agarose gel in 1× TAE buffer developed at 90 V for 30 min. Fresh gels were imaged on a Typhoon FLA9500 and quantified by densitometry using ImageQuant software. Each experiment was done in triplicate. It is important to note that despite the apparently low concentration of free Mg^{2+} resulting from the presence of ATP (estimated to be in the range of 30 μM in Yen1 reactions; K_D for ATP·Mg^{2+} is around 50 μM (57)), optimization experiments showed that under the described conditions, an optimal balance between D-loop formation and its subsequent processing by SSEs could be achieved (Supplementary Figure S1C).

When D1-3SP invading molecule was used, reactions were performed as described above, but increasing the final reaction volume to 25 μl. Then, 10 μl of each reaction was deproteinized and analysed on agarose gels. Another 10 μl was mixed with 1 vol of 2× denaturing loading buffer and incubated at 99°C for 3 min. Reaction products were then separated by 16% denaturing (7 M urea) PAGE gels in 1× TBE buffer. Gels were scanned on a Typhoon FLA9500 and quantified by densitometry using ImageQuant software.

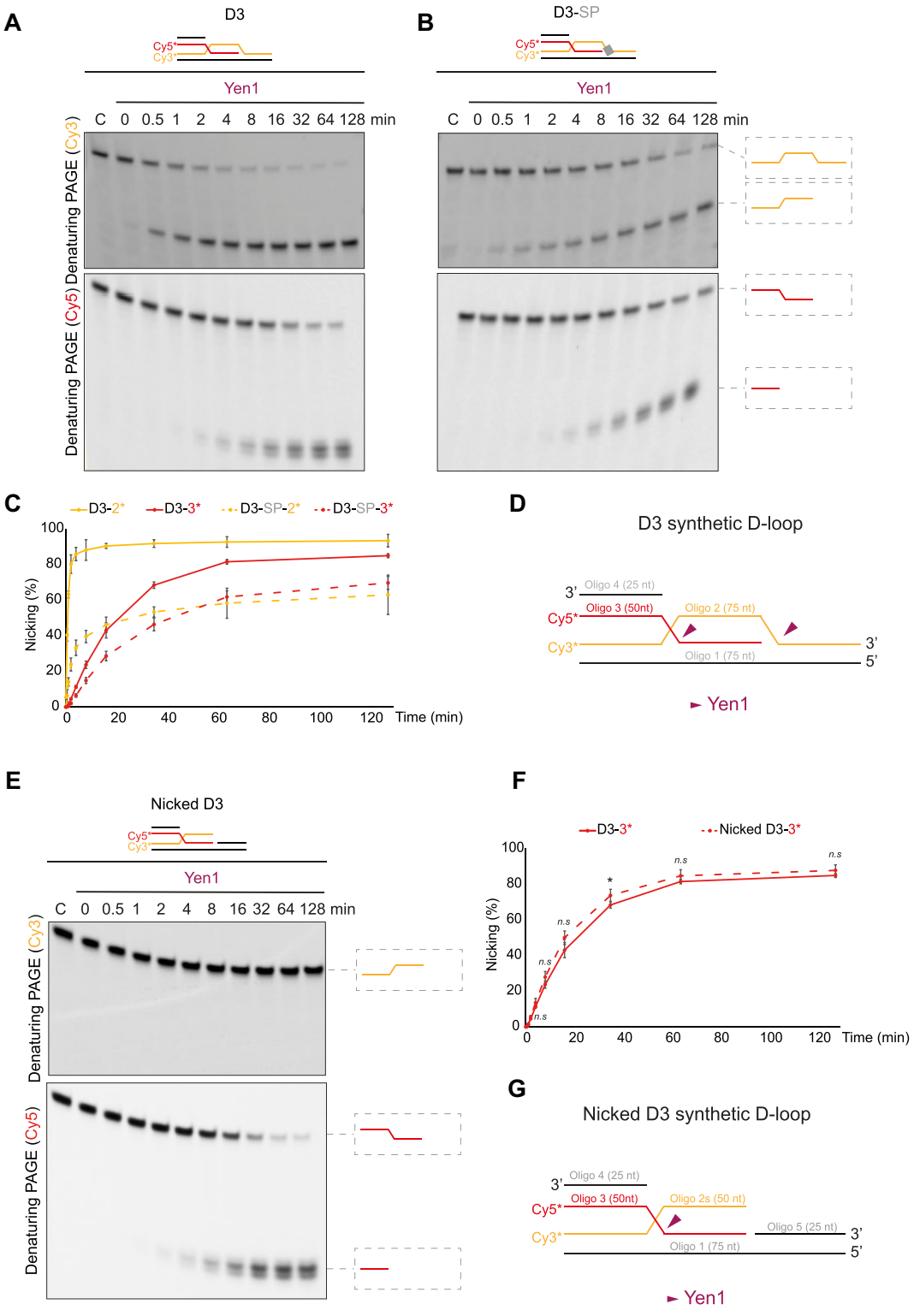

Figure 2. The two incisions produced by Yen1 on a D3 D-loop display different kinetics. (**A**) Time-course analysis of Yen1 cleavage on synthetic D3 D-loop: 10 nM D3 D-loop or (**B**) D3 D-loops with 3 hydrolysis-resistant phosphorothioate linkages (D3-SP, SP linkages in the oligo 2 are located between nt 50–51–52–53, depicted by a grey box) were incubated with 20 nM Yen1 for the indicated times at 30°C. The DNA substrates were labelled with Cy3 at the 5′-end of oligo 2 and with Cy5 at the 5′-end of oligo 3. The reaction products were analysed by 10% denaturing PAGE, scanned using a Typhoon FLA9500, and are depicted on the right. Representative gel images are shown. (**C**) Quantification of Yen1-mediated oligonucleotide nicking from denaturing PAGEs shown in (A) (solid lines) and (B) (dashed lines). Data are represented as mean values ± SD ($n = 3$). (**D**) Schematic representation of the fluorescent synthetic D3 D-loop structure. Yen1 incision sites are indicated by purple arrowheads. (**E**) Time-course analysis of Yen1 cleavage on nicked D3 D-loop. Reactions were carried out, labelled, and analysed as described in (A) and (B). (**F**) Quantification of Yen1-mediated oligonucleotide incision of D3 (solid lines) and nicked D3 (dashed lines) D-loop structure. Data are represented as mean values ± SD ($n = 3$). $P > 0.05$ (n.s.); $^*P < 0.05$. Student two-tailed *t*-test for samples with equal variance and the Welch *t*-test for samples with unequal variance. (**G**) Schematic representation of Yen1 incision (purple arrow) on a nicked D3 D-loop.

For experiments using the ExoSAP-IT enzyme (Thermo Fisher, #78201), 100 nM 90-nt 5′end-6FAM-labelled D1 oligo was incubated with 5 μl ExoSAP-IT at 37ºC the indicated times (0, 0.5, 1, 2, 4, 8, 16, 32, 64 min). Then, 5 μl of each reaction was deproteinized and mixed with 0.2 vol 6× glycerol loading buffer and analysed by electrophoresis in a 0.9% agarose gel in 1× TAE buffer developed at 90 V for 30 min. Another 5 μl was mixed with 1 vol of 2× denaturing loading buffer and incubated at 99ºC for 3 min. Reaction products were then separated by 16% denaturing (7 M urea) PAGE gels in 1× TBE buffer. Fresh gels were scanned in a Typhoon FLA9500.

RecA-mediated D-loops

RecA D-loops were generated in a similar way and in the same D-loop buffer as stated above, except in the presence of 15 mM $MgCl_2$. D1 oligonucleotide (40 nM) was incubated with 4 μM RecA for 5 min at 37ºC, followed by the addition of a single-stranded binding protein (100 nM SSB or RPA) when required. The reaction continued for an additional 5 min at 37ºC. D-loop formation was initiated by the incorporation of pBSK (1/5 total volume, 64 ng/μl final concentration) and, after 0.5 min, reactions were diluted 1:10 in Yen1 buffer (50 mM Tris–HCl pH 7.5) for Yen1 reactions or 1:5 in Mus81 buffer (25 mM Tris–HCl pH 7.5, 100 mM NaCl) for Mus81-Mms4 reactions, to reach, in both cases, the optimal $MgCl_2$ concentration for nuclease activity. One μl of each SSE (storage buffer for control reactions) was added at the indicated concentration and incubated for 5 min at 30ºC. Reactions were then deproteinized by addition of 2.5 μl STOP solution (0.1% SDS, 2 mg/ml PK) and incubation at 37ºC for 2 h. Analysis was performed as described above. Each experiment was done three independent times.

Deproteinized D-loops

Rad51/Rad54-mediated D-loop formation was carried out as previously described. Before SSE incorporation, half of the reaction was deproteinized by the addition of 0.75 μl STOP solution and incubation at 37ºC for 15 min. To remove PK and SDS, 1 vol of phenol–chloroform was added, followed by DNA precipitation with 2 vol of 100% EtOH, 0.1 vol of 3 M sodium acetate pH 5.2, and 0.02 vol of 5 mg/ml glycogen. Pellet was resuspended in the original volume in which the D-loop reaction had taken place. The deproteinized D-loops were then used in nuclease reactions, which were carried out and analysed as described above. After being scanned to visualize the fluorescent products, gels were stained with ethidium bromide (5 μl of 10 mg/ml ethidium bromide (EtBr) solution in 100 ml TAE) and imaged in a Gel Doc XR+ System using the Image Lab software (Bio-Rad). Each experiment was carried out in triplicate.

D-loops with a stable presynaptic filament

For experiments using the non-hydrolysable ATP analogue ATPγS, Rad51/Rad54-mediated D-loops were generated as described above, with the following modifications: 40 nM D1 oligonucleotide was incubated with Rad51 (2 μM) in D-loop buffer without the ATP regeneration system (creatine phosphate and creatine kinase) and with 2.5 mM ATPγS or ATP for 9 min at 37ºC, followed by addition of Rad54 (300 nM), 2.5 mM ATP, and incubation at 23ºC for 3 min. D-loop formation was initiated by the incorporation of pBSK (64 ng/μl final concentration), incubated for another 10 min at 23ºC, and analysed as previously described. All experiments were carried out in triplicate.

Mapping SSE cleavage sites on enzymatically generated D-loops

To map the cleavage sites in the invading molecule, Rad51/Rad54-mediated D-loop formation and treatment with the nucleases were done as described above, except in 25 μl total reaction volume. After nuclease incubation, 10 μl of each reaction were deproteinized and analysed on agarose gels as stated above, to monitor D-loop formation and nuclease activity. Another 10 μl aliquot was mixed with 1 vol of 2× denaturing loading buffer and incubated at 99ºC for 3 min. Reaction products were then separated by denaturing PAGE (7 M urea) in 1× TBE buffer. Gels were scanned on a Typhoon FLA9500 and quantified by densitometry using ImageQuant software.

To analyse the incision in the donor plasmid molecule (pBSK), Rad51/Rad54-mediated D-loop formation (20 μl final volume) and cleavage with the indicated nuclease (as described), was followed by cleavage with 10 U *Bsp*HI (New England Biolabs, #R0517S) and incubated at 37ºC for 20 min followed by dephosphorylation with 1 U Shrimp Alkaline Phosphatase (rSAP, New England Biolabs, #M0371S) and incubation for another 20 min. To verify D-loop formation and nuclease activity, half of each reaction was deproteinized and analysed on agarose gels as described above. The other half was denatured at 99ºC for 3 min, followed by labelling using 1 μl [γ-^{32}P]-ATP (3000 Ci/mmol) and 10 U T4 PNK for 1 h at 37ºC. The non-incorporated isotope was removed using G-25 columns (GE Healthcare) and the eluted DNA was precipitated with 2 vol of EtOH, 0.1 vol of 3 M sodium acetate pH 5.2 and 0.02 vol of 5 mg/ml glycogen. The pellet was resuspended in 10 μl 2× denaturing loading buffer and samples were analysed through denaturing PAGE, exposed to a phosphor screen, and visualized in a Typhoon FLA9500.

For mapping experiments using Sanger sequencing, after D-loop formation in 25 μl final volume and incubation with the indicated nuclease, each reaction was deproteinized by the addition of 3.75 μl STOP solution and incubation at 37ºC for 30 min. To verify D-loop formation and nuclease activity, 5 μl of the reaction were analysed on agarose gels. The rest of the reaction was adjusted to 75 μl with water, followed by addition of 1 vol of phenol-chloroform. After phenol–chloroform extraction, DNA precipitation was carried out with 2 vol of EtOH, 0.1 vol of 3 M sodium acetate pH 5.2, and 0.02 vol of 5 mg/ml glycogen. The pellet was resuspended in 22 μl 10 mM Tris–HCl pH 8.0. Finally, 10 μl were used for sequencing with the forward primer (SEQ-FW, from 1767 to 1784 bp) and the other 10 μl for sequencing with the reverse primer (SEQ-RV, from 2162 to 2177 bp) (Supplementary Table S1) in Stabvida laboratories.

Detection of half-crossover precursors

In experiments detecting the formation of half-crossover precursors, Rad51/Rad54-mediated D-loop formation was performed in 1.5 mM $MgCl_2$ D-loop buffer, followed by simultaneous addition of 100 nM of both endonucleases and incubated for 1 h at 30ºC. When appropriate, 5 U of T4 ligase (Thermo Fisher, #EL0011) was added and incubated for 1 h at 23ºC. Then, 20 U of either *Eco*RV (EV, Thermo Fisher, #FD0304) or *Abd*I (AI, New England Biolabs, #R0584S) was

included and incubated at 37°C for 1 h. After treatment with the restriction enzymes, reactions were deproteinized, analysed by agarose gel, scanned in a Typhoon FLA9500, and stained with EtBr as stated above. For analysis by denaturing PAGE (using 7 M urea), after the cleavage with restriction enzymes, reactions were mixed with 1 vol of 2× denaturing loading buffer and incubated at 99°C for 3 min. Reaction products were then separated by denaturing PAGE in 1× TBE buffer and fresh gels were scanned on a Typhoon FLA9500.

Yeast strains and methods

The *S. cerevisiae* strains used in this study are described in Supplementary Table S3. All routine manipulations were performed following standard procedures (58).

Deletions of *MUS81*, *MMS4*, and *YEN1* were generated by PCR-based gene replacement using *natNT2*, *hphMX4*, *hphMX6*, or *LEU2* as selection markers (59,60). The coding sequences of both untagged and tagged versions of *MUS81*, *MMS4* and *YEN1* were cloned under the control of their endogenous promoter in pRSII405 or pRSII406 (61) to generate pRSII405-*MUS81*, pRSII405-3xFLAG-*MUS81*, pRS406II-*MMS4*, pRS406II-10xHIS-StrepII-*MMS4*, pRS406II-*YEN1*, and pRS406II-*YEN1*-3xFLAG-2xTEV-10xHIS. Next, the vectors were linearized for integration at the endogenous *leu2* (pRS405II derivatives) or *ura3* (pRSII406 derivatives) loci in the appropriate mutant yeast strains. DNA-damage sensitivity assays were carried out as previously described (62).

Statistical analyses

Unless indicated otherwise, data is presented as the mean of three independent experiments ± SD. Statistical analysis was performed using the student two-tailed T-test for samples with equal variance and the Welch *t*-test for samples with unequal variance. A *P*-value >0.05 was considered statistically not significant (n.s.); $*P < 0.05$, $**P < 0.01$, $***P < 0.001$, $****P < 0.0001$. Graphs were created in Microsoft Excel.

Results

Both Mus81 and Yen1 can cleave oligonucleotide-based D-loops

To compare the ability of Yen1 and Mus81 to process synthetic D-loops, we incubated purified proteins with three different oligo-based D-loop structures (D3, D2, D1, Supplementary Table S2). These substrates were 5′-^{32}P-end-labelled on one strand, and the reaction products were analysed using native and denaturing PAGE (Figure 1 and Supplementary Figure S2). As these three structures have two branching points, the one at the 5′-side of the invading strand will be referred to as the first branching point and the other one as the second branching point. For the synthetic oligonucleotide-based molecule that recapitulates the nascent D-loop intermediate (D3 D-loops), Mus81 exhibited multiple cuts (position 41–47) on the strand complementary to the invading molecule (oligo 1, Figure 1A–D) as expected from previous studies (43,44,50,63). The predominant incision occurred 5 nt from the 5′-side of the first branching point (Figure 1C, D). Yen1 incisions mapping showed that it can cleave all four strands within the D3 D-loop, albeit with different efficiency. The displaced strand (oligo 2) was predominantly cleaved from nt 51 to 53, with the main incision at position 51, which is 1 nt from the 3′-side of the second branching point (Figure 1C, D). Yen1 could also nick the invading molecule (oligo 3) at 1 to 3 nt from the first branching point. Some nucleolytic activity was detected at the 5′-end of the strand complementary to the invading oligo (oligo 4), explaining the loss of labelling on the native gel (Figure 1A). Importantly, these activities were absent when the nuclease-dead mutants (ND) were used. Further analysis using a shorter oligo 4 (oligo 4s) confirmed that Yen1's activity on the 5′-end depends on the proximity of the 5′-phosphate group to the invasion point (Supplementary Figure S2A–C).

Two additional D-loop structures were generated: the D2 D-loop, characterized by a fully ssDNA 5′-overhang in the invading oligo, which mimics the scenario after D-loop bubble migration (Figure 1E), and the D1 D-loop, a widely used structure for studying recombination intermediates *in vitro* (9,13,16,17,26,55,64), where the invading strand has no overhangs (Figure 1F). Yen1 cleaved the D2 D-loop at equivalent positions to D3, while Mus81 was unable to process it (Figure 1E and Supplementary Figure S2D-E). In the case of D1 D-loop, both Mus81 and Yen1 cleaved the displaced strand at the branching point. Mus81 predominantly nicked the D1 substrate at position 25 (first branching point), while Yen1 cleaved it 1 nt from the 3′ side of the second branching point (Figure 1F and Supplementary Figure S2F, G). Collectively, these results showed that both Yen1 and Mus81 can process oligonucleotide-based D-loop structures according to their respective polarities. Notably, the main incision produced by Mus81 in combination with Yen1's incision at the end of the displaced strand in the D3 structure is compatible with the generation of a HC outcome in the context of BIR repair (Supplementary Figure S3A). Moreover, Yen1's cleavage at the invading strand could contribute to the generation of CL events in a BIR scenario (Supplementary Figure S3B).

Yen1 incision of the displaced strand in D3 D-loops may facilitate the processing of the invading strand

As Yen1 can cut both the invading and the displaced strands within the D3 structure, we aimed to determine if the two predominant Yen1 incisions observed in this structure were co-dependent or could be uncoupled. Time-course analyses of D3 cleavage by Yen1 revealed that processing of the displaced strand occurred faster than that of the invading one (Figure 2A, C, and D). To investigate if the processing of the invading oligo requires prior incision of the displaced strand, we introduced three phosphorothioate linkages between the nucleotides 50–53 of the oligo 2 to inhibit Yen1 cleavage on the displaced strand. This modification resulted in an approximately 50% reduction in Yen1 activity on the displaced strand (Figure 2B) but led to only ∼25% decrease in incisions on the invading oligo (Figure 2C). These findings suggested that the two incisions were not inherently coupled. To further confirm this observation, we created a D3 D-loop with a nicked displaced strand that mimics Yen1 incision. If cleavage of the invading strand by Yen1 depended on the initial incision, it should be enhanced with this substrate. However, the cleavage kinetics of the invading strand using both nicked and intact D3 D-loops were very similar (Figure 2E–G). Altogether, these results suggest that while the cleavage of the invading oligo 3 may be facilitated by increased substrate flexibility after incision of the displaced oligo 2, it is not its prerequisite.

Mus81 and Yen1 can cleave Rad51/Rad54-mediated D-loops

Next, we aimed to address whether Yen1 and Mus81 can also process more physiological D-loops, decorated by the recombination machinery, which may sterically impair nuclease accessibility. For this reason, we reconstituted D-loop formation using purified yeast Rad51 and Rad54 (Supplementary Figure S4A), the negatively supercoiled plasmid (pBSK) as a donor molecule, and a fully homologous 6FAM 5′-labelled 90 nt ssDNA (D1) as an invading DNA (55) (Figure 3A). After D-loop formation, Yen1 or Mus81 were added, and 15 min later, reactions were stopped, and D-loop processing was analysed by agarose gel electrophoresis. Both enzymes exhibited dose- and catalysis-dependent destabilization of the Rad51-mediated D-loop (Figure 3B), indicating their nucleolytic processing. In Yen1 reactions, a smear dependent on nuclease activity was observed migrating above the free-oligonucleotide band. Considering the exonucleolytic activity detected at the invading oligo in the D1 synthetic D-loop (Figure 1F), we speculated that this band could result from Yen1 cleaving the 5′-end of the invading strand. This would release 5′-labelled mono-, di-, or oligonucleotides with abnormally slow electrophoretic mobility, as observed with other fluorochromes (65). To test this hypothesis, we generated a D1 D-loop using an invading oligonucleotide with three hydrolysis-resistant SP linkages at the 5′-end and incubated it with Yen1 (Supplementary Figure S4B). In native agarose gels, we observed a slight decrease in the formation of the diffuse band compared to the unmodified D1 D-loop, while denaturing PAGE analysis revealed short cleavage products (5–7 nt) when either substrate was used (Supplementary Figure S4C-D). This suggests that, rather than an exonuclease activity, this smear band might arise from incomplete invasions of the D1 oligonucleotide, leaving short unpaired 5′-ssDNA overhangs that Yen1 could recognize and process as a 5′-flap structure (66). Additionally, we independently confirmed that 6FAM 5′-labelled short oligonucleotides produced by a 3′-5′exonuclease activity on the 90-nt D1 oligonucleotide display slower electrophoretic migration in agarose gels than the full-length molecule (Supplementary Figure S4E, F). In addition, to create a more physiological situation, we enzymatically generated two additional D-loops: D2 (with a 5′-ssDNA non-homologous overhang) and D3 (with a 5′-dsDNA non-homologous overhang), which more closely mimic D-loops generated *in vivo*. While Yen1 was able to process both D2 and D3 structures, Mus81 could only act on D3 (Figure 3C,D), consistent with their processing of the synthetic structures (Figure 1). In summary, these experiments demonstrate that both Yen1 and Mus81 can process plasmid-based D-loops decorated with the proteins responsible for their formation *in vivo*.

Mus81 and Yen1 cleave Rad51-mediated D-loops coated by RPA

Another protein implicated in D-loop formation in cells is the heterotrimeric ssDNA binding protein RPA. *In vitro*, RPA stabilizes D-loops by binding to the displaced strand and preventing its reannealing to the template strand (67,68). To test if RPA could influence D-loop cleavage by the SSEs, we generated D1 D-loops in the presence or absence of RPA and used them as substrates for the endonucleases (Figure 4A). As shown in Figure 4B, Yen1 cleaves the D1 D-loop with equal efficiency regardless of the presence of RPA. In the case of Mus81, rather than preventing cleavage, RPA seems to significantly enhance Mus81 cleavage of the D1 structure (Figure 4C). Similar experiments with D2 and D3 D-loops confirmed that RPA has no effect on Yen1 activity and mild effect on Mus81 activity on the D3 structure (Figure 4D–G). To determine if RPA stimulates Mus81 on a simpler substrate, we used a 3′-flap structure with a long ssDNA tail (80 nt) that was pre-incubated for 10 min with increasing concentrations of RPA before adding Mus81 to the reaction. Increasing concentration of RPA inhibited Mus81 activity on this substrate (Supplementary Figure S5A). Importantly, when the same concentration of RPA as used in the D-loop reactions was employed (600 nM), almost no cleavage was detected. This indicates that RPA not only does not stimulate Mus81 activity on one of its preferred substrates but rather inhibits its nuclease activity, suggesting that the observed stimulation of D-loop cleavage might reflect different binding or coordination with RPA. We next addressed if the presence of another single-stranded binding protein on the D1 substrate could stimulate Mus81 activity. To explore this possibility, we performed similar D-loop cleavage assays using the bacterial ortholog of RPA, *E. coli* SSB (Supplementary Figure S5B). As shown in the Supplementary Figure S5C-D, the presence of SSB did not alter the ability of Mus81 or Yen1 to process D1 D-loops. Therefore, to assess if the stimulatory effect of RPA on Mus81 cleavage might depend on the presence of Rad51, we generated D1 D-loops using the bacterial ortholog of Rad51, RecA and subsequently incubated them with SSB or RPA, prior to nuclease incorporation. While both Mus81 and Yen1 were able to process D1 D-loops generated with RecA, no significant differences were observed when either SSB or RPA were used (Supplementary Figure S5E–H). Collectively, these results indicate that neither the presence of RPA nor its bacterial ortholog SSB prevent nuclease activity on the recombination intermediates generated *in vitro*. Furthermore, we have shown that although with very different efficiency, both Yen1 and Mus81 can process RecA-mediated D-loop structures.

D-loop proteins impair nuclease cleavage and Rad51 turnover facilitates SSEs activity

Given our previous results, we wanted to investigate if the same proteins required for D-loop formation could modulate the accessibility of the nucleases to the recombination intermediates. To address this, we examined the effect of deproteinization of Rad51/Rad54-coated D1 structures before Yen1 or Mus81 treatment (Supplementary Figure S6A). Under identical nuclease concentration, total amount of DNA, and proportion of D-loop formation, both Yen1 and Mus81 displayed faster cleavage kinetics with deproteinized D-loops compared to coated ones (Supplementary Figure S6B, C). This observation indicates that Rad51 and Rad54 restrict the accessibility of the SSEs to these structures. If the higher efficiency of Yen1 and Mus81 in processing deproteinized D-loops is due to the protective effect of Rad51 and Rad54 proteins, one would predict that generating D-loops with a more stable nucleofilament should reduce accessibility to the nucleases and their catalytic activity. Previous studies have demonstrated that the use of the slowly hydrolysable ATP analogue, ATPγS, leads to a reduction in the efficient turnover of the Rad51–dsDNA complex (69). We therefore assembled a more stable nucleofilament by incubating Rad51 with ATPγS followed by ATP

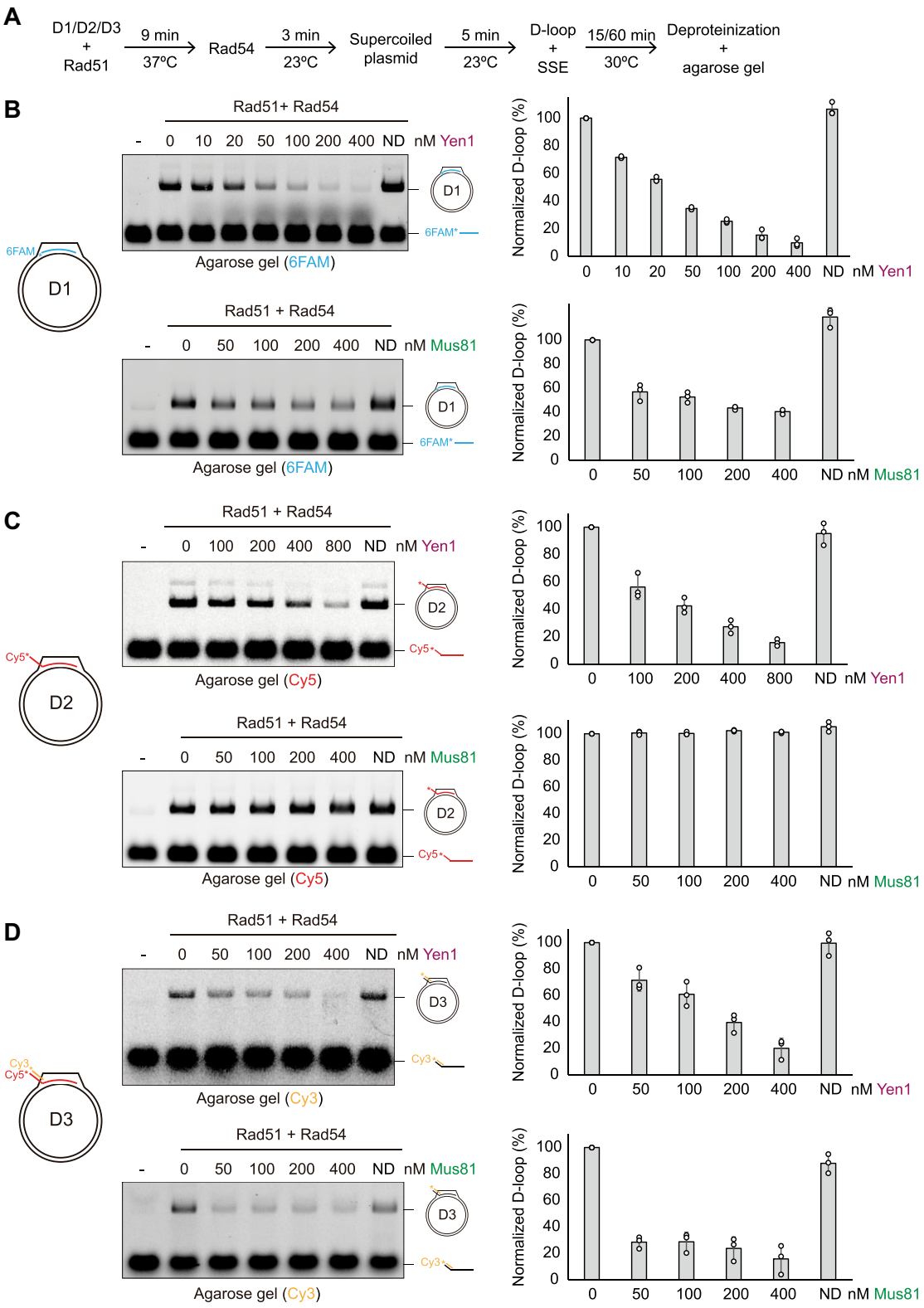

Figure 3. Yen1 and Mus81 process Rad51-mediated D-loops. (**A**) Scheme for Rad51/Rad54-mediated D-loop reaction: End-labelled DNA substrates (40 nM) were incubated with Rad51 (2 μM) at 37°C for 9 min. Rad54 (300 nM) was then added to the reaction and incubated for 3 min at 23°C. Subsequently, supercoiled pBSK (640 ng) was added and incubated for another 5 min before incorporation of SSE. After 15 min incubation with either nuclease at 30°C, the reactions were deproteinized and analysed on agarose gels. (**B**) Representative agarose gel from reactions with enzymatic D1 D-loop treated with Yen1 (top) or Mus81 (bottom). The absence of nuclease is indicated by (-). Nuclease-dead mutant controls (ND) were performed at the highest concentration of the wild-type enzymes. The gels were scanned and quantification of D1 D-loop cleavage by the SSEs is shown on the right. The D-loops were normalized by setting the initial D-loop yield as 100%. The data are plotted as means ± SD ($n = 3$). White circles represent individual values. A graphical representation of a plasmid-based D1 D-loop is shown on the left. Please note that the fuzzy band above the free 6FAM-labelled oligonucleotide corresponds to small 6FAM-labelled ssDNA products generated by Yen1 exonuclease activity. (**C**) Same as (B) but using the enzymatic D2 D-loop. (**D**) Same as (B) but using the enzymatic D3 D-loop and 60 min for SSE incubation.

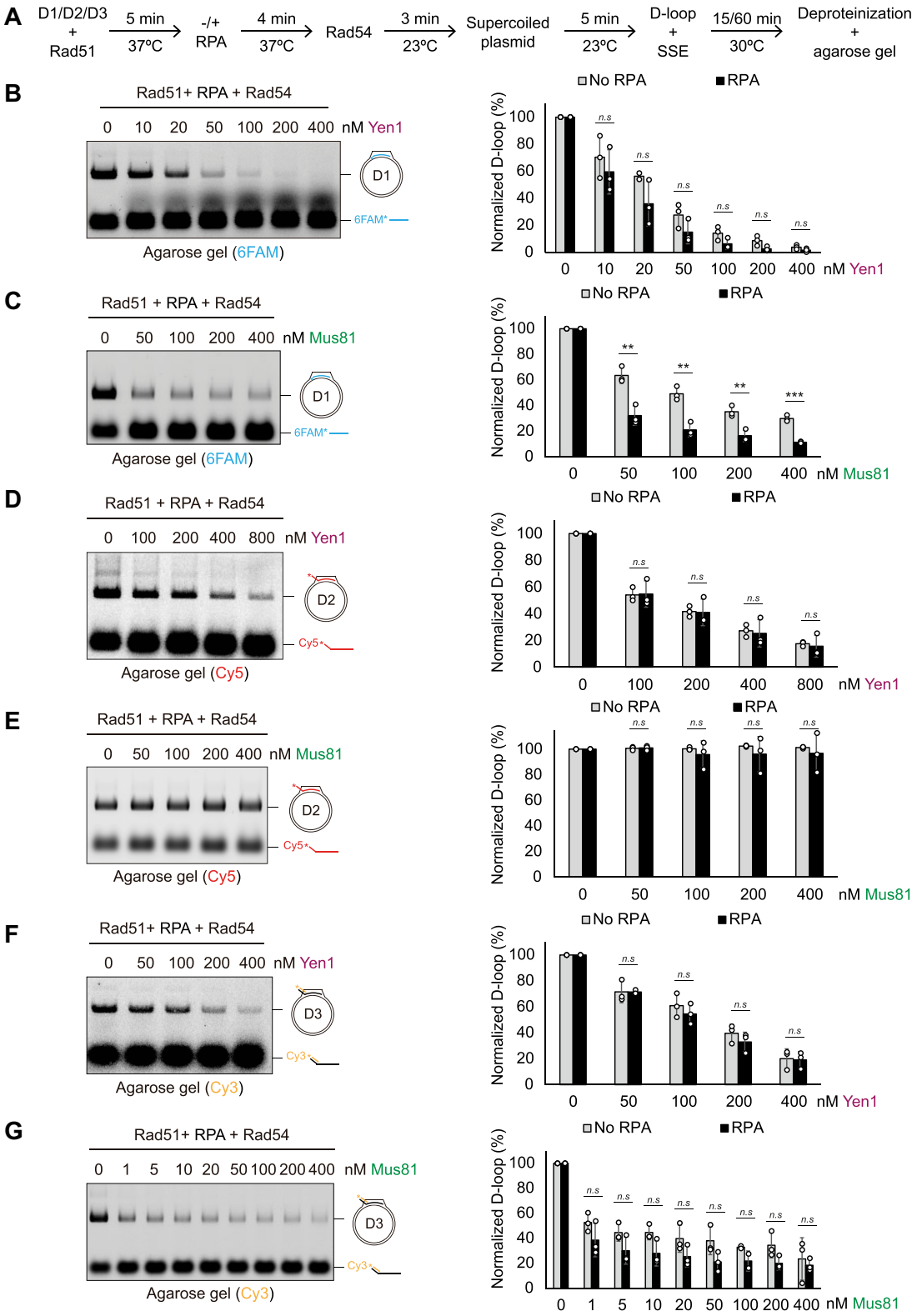

Figure 4. Effect of RPA on D-loop cleavage by SSEs. (**A**) Experimental scheme of Rad51/Rad54-mediated D-loop reactions with RPA. 5′-end-labelled D1 or D3 molecules (40 nM) were incubated with Rad51 (2 μM) at 37°C for 5 min. When appropriate, RPA (600 nM) was added and incubated for 4 min at 37°C. Then, Rad54 (300 nM) was added to the reaction and incubated for 3 min at 23°C, followed by incorporation of supercoiled pBSK (640 ng) and incubation at 23°C for 5 min. The indicated SSE concentrations were added, and reactions were further incubated at 30°C for 15 min for D1 D-loop or 60 min for D3 D-loops. (**B**) Representative agarose gel from reactions with Yen1 and enzymatic D1 D-loops with RPA. Graphs represent the quantification of D-loop cleavage by Yen1. D-loops were normalized by setting the initial D-loop yield as 100% and plotted as means ± SD ($n = 3$). $P > 0.05$ (n.s.); $^{*}P < 0.05$; $^{**}P < 0.01$; $^{***}P < 0.001$. Student two-tailed *t*-test for samples with equal variance and the Welch *t*-test for samples with unequal variance. White circles represent individual values. (**C**) Same as (B) but using Mus81. (**D**, **E**) Same as (B) and (C) but for D2 D-loop substrate. (**F**, **G**) Same as (B) and (C) but for D3 D-loop substrate.

incorporation, upon addition of Rad54 to the reaction (Figure 5A). As depicted in Figure 5B, D-loop formation was nearly abolished when only ATPγS was used, but restored by incorporation of ATP together with Rad54. Using this strategy, we performed kinetic analyses to examine if the slow turnover of Rad51 in the presynaptic filament could interfere with nuclease cleavage (Figure 5C). Indeed, the stabilization of the Rad51 nucleofilament using ATPγS strongly reduced the ability of both Yen1 and Mus81 to process D-loop structures (Figure 5D, E). Taken together, these results indicate that the status of Rad51 nucleoprotein could play a regulatory role against the nucleolytic processing of D-loops by Yen1 and Mus81.

SSEs incisions on enzymatically made D-loops map at similar positions to those on synthetic D-loops

To address whether the presence of Rad51/Rad54 and RPA not only affects the efficiency of D-loop processing, but also influences the location of incisions produced by these SSEs, we developed a methodology to map their cleavage sites on the plasmid-based D-loops (Figure 6A). Initially, we focused on the D3 structure and assessed whether the nucleases cleaved the invading strand. After D-loop formation and incubation with Yen1 or Mus81, the reaction products were separated using denaturing PAGE and scanned for Cy5 (invading strand) and Cy3 (complementary oligo in the non-invading duplex region). Yen1 generated a major incision at nt 25 in the 5′-Cy5-labelled invading strand, 5 nt downstream from the beginning of the homology region (Figure 6B). In addition, several secondary incisions were observed ranging in size from 22 to 40 nt, approximately 20 nt after the start of the homology region (Figure 6B). This ladder of incisions could be attributed to the dynamics of the D-loop formation process, with Yen1 cleaving the 5′-overhang near the branching point, as observed for the D1 structures (Supplementary Figure S4D). In contrast, analysis of the cleavage pattern of the 3′-Cy3-labelled oligo revealed no activity (Figure 6B). Similarly, no activity was detected for Mus81 on neither the invading oligo nor its complementary strand (Figure 6C), consistent with the results obtained using the synthetic D3 structure (Figure 1).

To determine whether these nucleases were cleaving the plasmid, we treated D3 D-loop reaction products of Yen1 or Mus81 with *Bsp*HI (Figure 6A, black arrowhead). Given the position of the homology region between the invading oligo and pBSK, an incision by Yen1 at the end of the displaced strand combined with *Bsp*HI treatment should release a fragment of approximately 140 nt that could be detected after radioactive labelling and separation by denaturing PAGE (Figure 6A). Accordingly, only the reactions treated with Yen1 and *Bsp*HI displayed bands near the expected sizes (approx. 140 and 130 nt) (Figure 6D). Similarly, we confirmed that the combined processing of the D3 substrate by Mus81 and *Bsp*HI released a specific fragment of approximately 60 nt, which corresponds to Mus81 incising the template strand of the plasmid at equivalent positions to the synthetic D3 D-loop (Figure 6A and E). A limitation of this strategy is its inability to distinguish incisions generated at the expected positions on either strand of the plasmid, as they would release DNA fragments of the same size in combination with *Bsp*HI. Therefore, we complemented these experiments with an alternative mapping approach by utilizing the untemplated addition of an adenine nucleotide by *Taq* polymerase at the 3′-end of DNA strands in sequencing reactions (Supplementary Figure S7A). Consequently, sequencing DNA from SSE-treated D-loop reactions revealed novel A peaks or peaks of increased intensity only in the nicked strand, allowing the determination of the strand cleaved by Yen1 and Mus81 with single-nucleotide resolution. As expected, Yen1 cleaved the D3 D-loop at the end of the displaced strand, while Mus81 incised the template strand 4–5 nt upstream of the start of the invasion region, consistent with our observations using the synthetic D3 substrate (Figure 6F and Supplementary Figure S7B). To confirm the specificity of the sequencing results, we conducted similar experiments with a different D3 D-loop structure (D3.2), in which the homologous region between the invading strand and pBSK was located at different position (Supplementary Table S2). The sequencing results demonstrated a shift in the A peaks to equivalent positions of the new D3.2 D-loop structure (Supplementary Figure S7C), thereby validating the mapping approach. The same methodology was applied to determine the incision sites created by Mus81 and Yen1 on D2 and D1 D-loops, respectively (Figure 6G and H). In the case of the D2 substrate, Yen1 activity resembled its activity on the D3 D-loop, exhibiting multiple cuts on the invading strand and cleaving the displaced strand at the other end of the D-loop (Figure 6G and Supplementary Figure S8A–D). Further confirmation of the specificity was obtained using a derivate D2 D-loop (D2.2, Supplementary Table S2), in which the 3′-end of the invading strand was located at different position within pBSK, resulting in a corresponding shift in the sequencing results (Supplementary Figure S8E). Regarding the D1 D-loop, Yen1 incisions on the displaced strand were consistent with those observed for D2 and D3. However, Mus81 shifted its activity to the displaced strand, cleaving 5–8 nt upstream of the 5′-end of the homology region (Figure 6H and Supplementary Figure S9A–F), consistent with the findings obtained with synthetic substrates. To confirm the mapping of the Mus81 incision, an additional D1 oligo (D1.2, Supplementary Table S1) was used, in which the 5′-invasion point was again moved to a different position within pBSK (Supplementary Figure S9G). Altogether, these results suggest that while the Rad51/Rad54 complex involved in D-loop formation may modulate the accessibility of the nucleases to these structures, its presence does not significantly alter their cleavage specificity compared to the naked, oligonucleotide-based D-loops. Furthermore, the newly developed mapping approach enabled precise determination of the incision sites and provided insight into the cleavage preferences of Yen1 and Mus81 during D-loop processing.

Concurrent cleavage of Mus81 and Yen1 on a plasmid-based D3 D-loop leads to a half-crossover precursor

Our mapping experiments demonstrate that Yen1 and Mus81 can introduce incisions on a D3 D-loop that are consistent with the predicted formation of half-crossovers, based on previous genetic studies (Supplementary Figure S3A) (28,35,37). Therefore, we next aimed to investigate if the combined activity of these two enzymes could generate such recombination product (Figure 7A). Surprisingly, when both Mus81 and Yen1 were present simultaneously, a fraction of the D-loop exhibited a shift to a slower migrating band instead of being destabilized (Figure 7B, arrow). Importantly, the appearance of this new product was dependent on the catalytic activity of both enzymes (Figure 7C). The reduced migration observed is

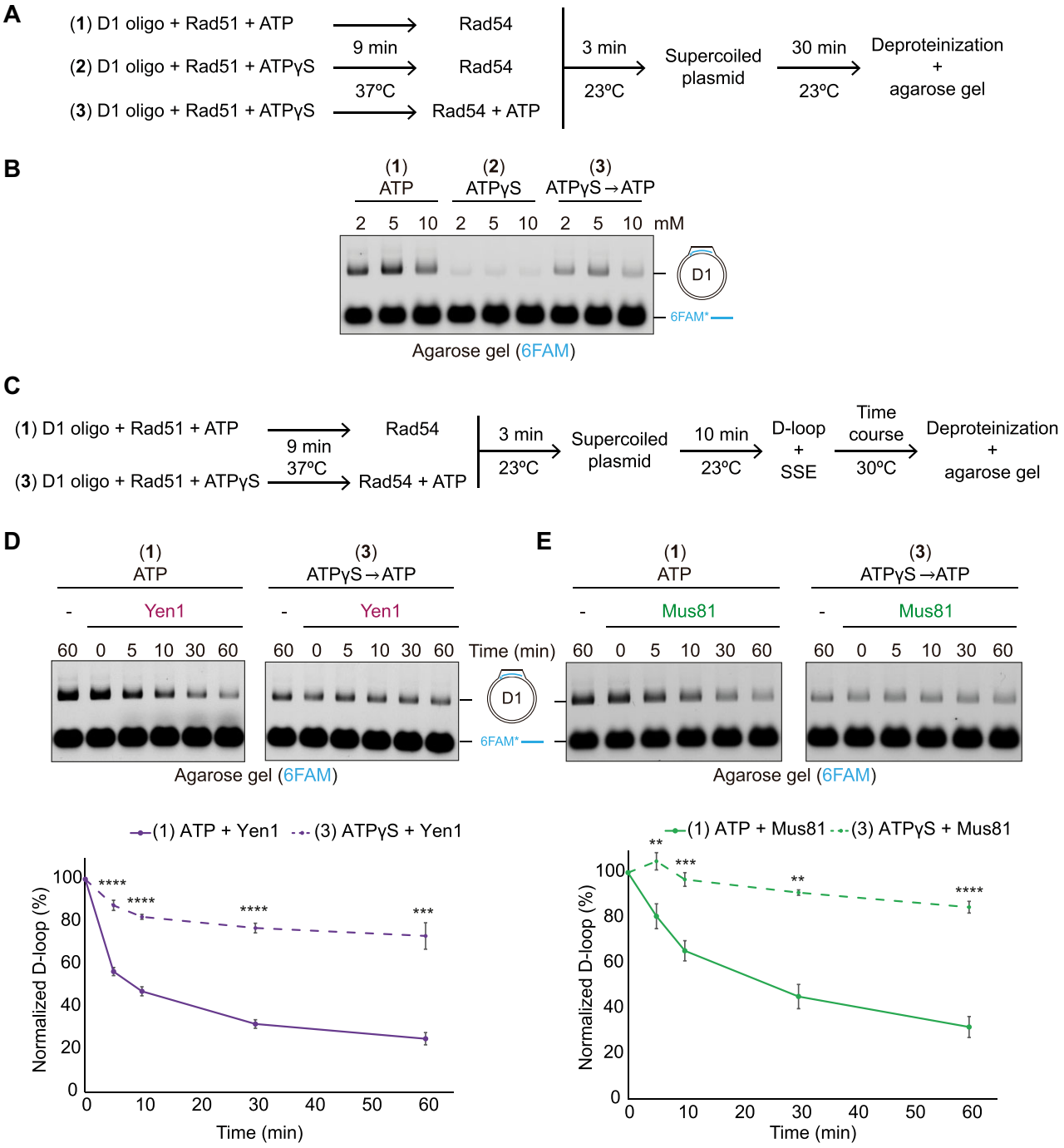

Figure 5. Effect of Rad51 nucleofilament stabilization on nuclease cleavage. (**A**) Experimental scheme of D1 D-loop reactions with the nucleofilaments generated in the presence of ATP (1), ATPγS (2), or ATPγS followed by ATP incorporation (3). 5′-6FAM-labelled D1 oligo (40 nM) was incubated with Rad51 (2 μM) in presence of either ATP or ATPγS at 37ºC for 9 min. Then, Rad54 (300 nM) was added, and in reaction number 3, where ATPγS was used, ATP was incorporated to enable Rad54 activity. Reactions were incubated for 3 min at 23ºC. Subsequently, supercoiled pBSK (640 ng) was added and incubated for 30 min at 23ºC prior to deproteinization and agarose gel analysis. (**B**) Representative gel of nucleotide effect (2, 5, 10 mM) on D1 D-loop formation in the presence of ATP (1), ATPγS (2), or ATP/ ATPγS (3). Note that when both adenosine nucleotides were used, half of each nucleotide was added to reach the indicated concentration. (**C**) Experimental scheme of nuclease reactions on D1 D-loops with the nucleofilaments generated in the presence of ATP (1) or ATPγS followed by ATP incorporation (3). Reactions were carried out as stated above. (**D**) Representative agarose gels showing time-course analyses of Yen1 (400 nM) activity on D1 D-loops generated in the presence of ATP (1) (left) or ATPγS/ATP (3) (right). (-) indicates no nuclease. Graph (bottom) represents the quantification of D-loop cleavage by Yen1. D-loops were normalized by setting the initial D-loop yield as 100%. Plotted are means ± SD ($n = 3$). $P > 0.05$ (n.s.); $^{*}P < 0.05$; $^{**}P < 0.01$; $^{***}P < 0.001$; $^{****}P < 0.0001$. Student two-tailed *t*-test for samples with equal variance and the Welch *t*-test for samples with unequal variance. Solid line: nucleofilament generated in the presence of ATP. Dashed line: nucleofilament generated in the presence of ATPγS. (**E**) Same as (D) but using Mus81 (400 nM).

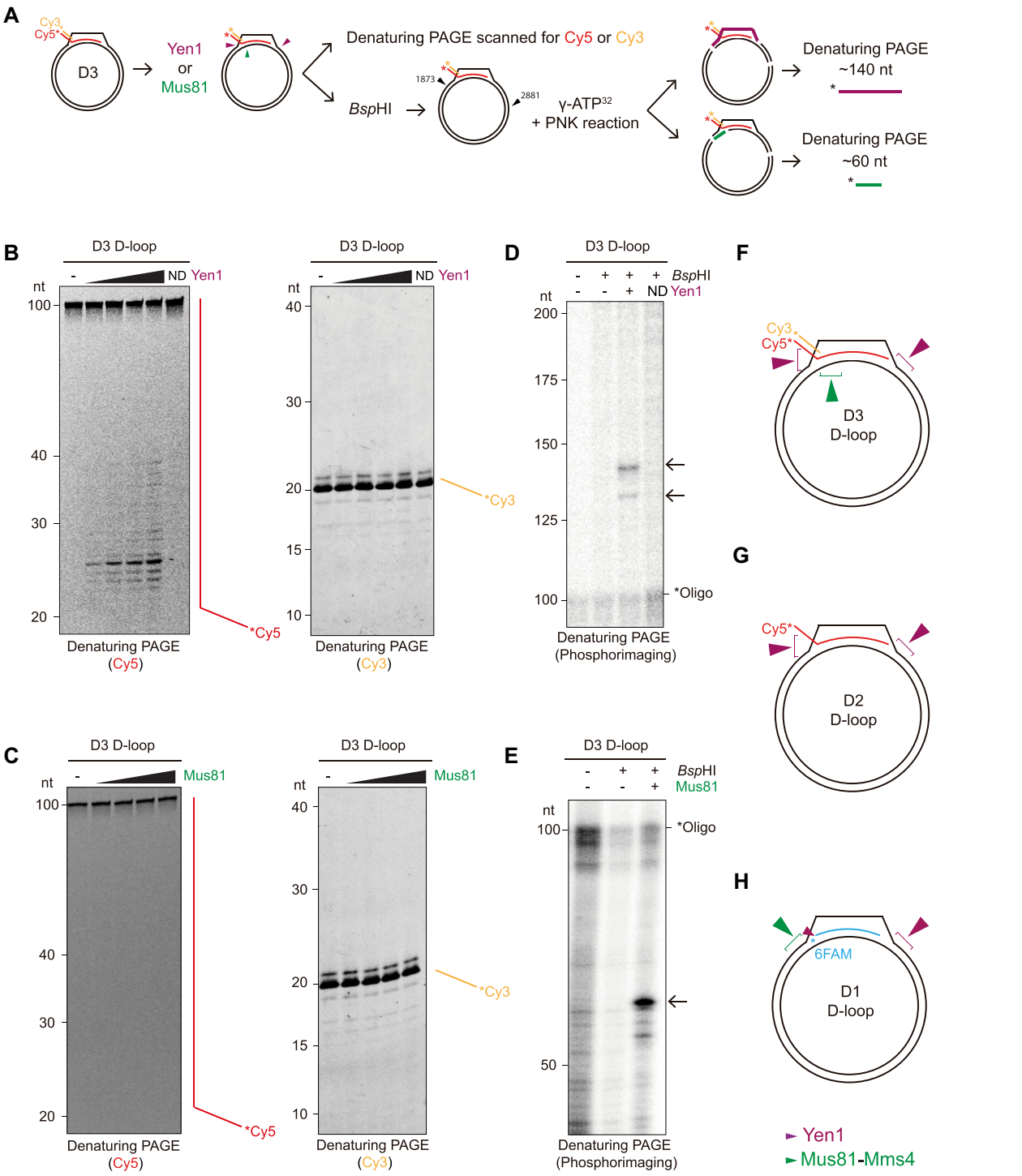

Figure 6. Mapping the D-loop cleavage sites of Yen1 and Mus81. (**A**) Mapping strategy for the D3 D-loop structure. The invading oligo is homologous to positions 1932 to 2012 of pBSK. After D3 D-loop formation, SSE activity on the invading molecule was analysed by fluorescence scanning after denaturing PAGE; SSE activity on the plasmid was analysed after *Bsp*HI treatment, radioactive labelling, and analysis on denaturing PAGE by phosphorimaging. (**B**) To identify cuts in the invading molecule, increasing concentrations of Yen1 (50, 100, 200, 400 nM) or 400 nM $Yen1^{ND}$ (ND) were added to the reaction after D3 D-loop formation and incubated for 1 h at 30°C. (–) indicates no enzyme. Reaction products were analysed by 12% denaturing PAGE and scanned. A mixture of 5′-6FAM-end-labelled oligos of defined length was used as marker. (**C**) Same as (B), but using increasing concentrations of Mus81 (50, 100, 200, 400 nM). (**D**) To identify incisions in the plasmid after D3 D-loop formation, 400 nM Yen1 was added to the reaction and incubated for 1 h at 30°C. Then, pBSK was digested with 10 U *Bsp*HI at 37°C for 20 min, followed by treatment with rSAP for another 20 min at 37°C and heat inactivation at 99°C for 5 min. Reaction products were labelled using T4 PNK and ^{32}P-γ-ATP and analysed by 6% denaturing PAGE followed by phosphorimaging. A mixture of DNA fragments was radioactively labelled and used as marker. Arrows indicate products of expected sizes. (**E**) Same as (D) but using 400 nM Mus81. Note: due to technical reasons, the catalytically inactive Mus81 version could not be included in this experiment, but the absence of contaminating nucleases in Mus81 preps has been evidenced elsewhere (Figures 1A and C, 3B-D, 7C, and Supplementary Figures S2, S5F, S7, and S9F). (**F**) Schematic representation of Yen1 (purple) and Mus81 (green) incisions on the plasmid-based D3 D-loop. (**G**) Same as (F) but for D2 D-loop substrate. (**H**) Same as (F) but for D1 D-loop substrate.

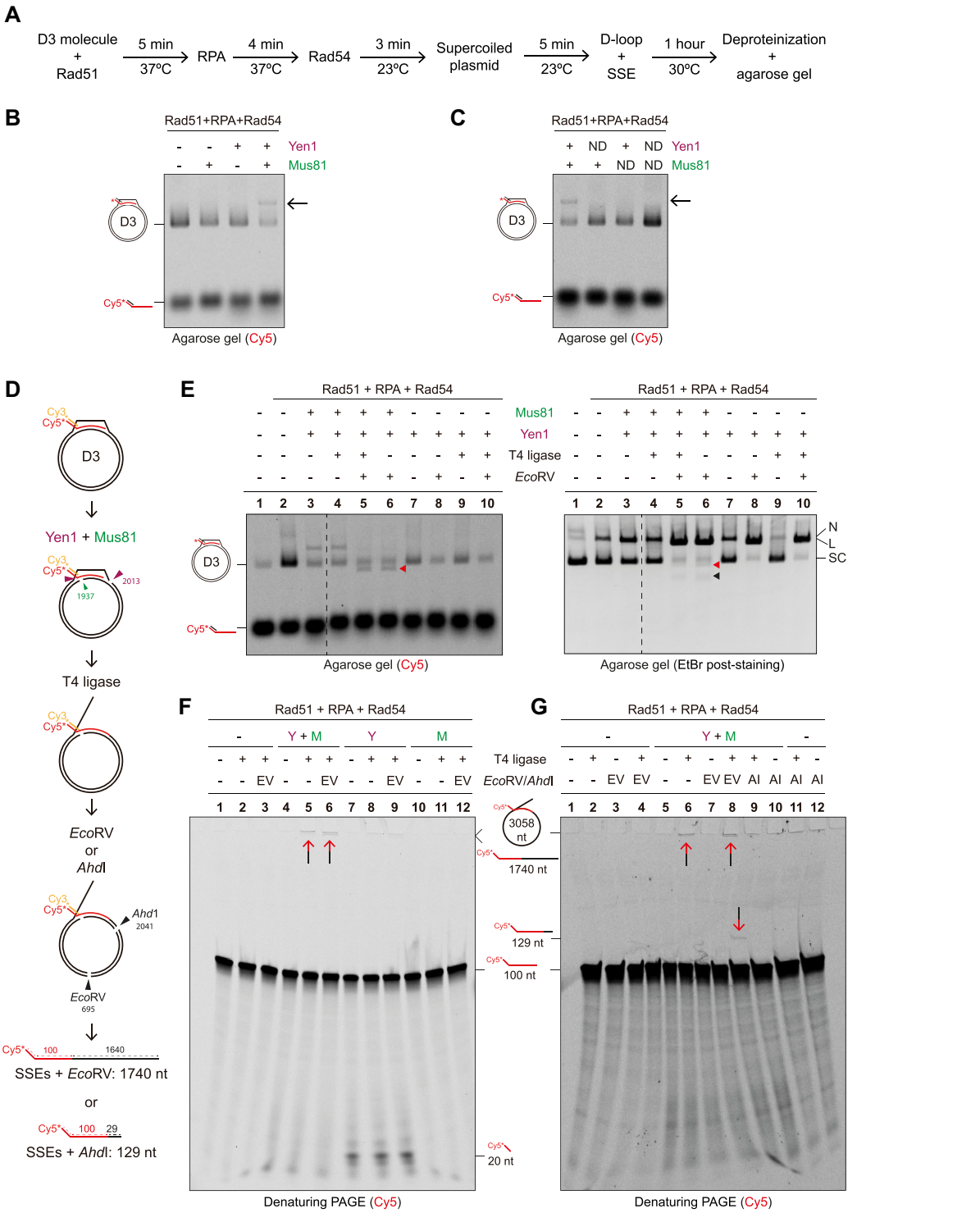

Figure 7. Detection of a half-crossover precursor by concurrent cleavage of D3 D-loop by Mus81 and Yen1. (**A**) Experimental scheme of Rad51-mediated D3 D-loop formation followed by Mus81 and Yen1 resolution. (**B**) Mus81, Yen1, or both were incubated with the D3 D-loop for 1 h at 30ºC, resolved on agarose gels, and scanned. (–) indicates no nuclease. Arrow indicates product of concurrent cleavage by Yen1 and Mus81. (**C**) Same as (B) except nuclease-dead mutants (ND) were used as controls. (**D**) Graphical experimental strategy to detect half-crossover precursors. After D3 D-loop cleavage with Yen1 and Mus81, reaction products were ligated using T4 ligase (1 h, 23ºC) and/or cleaved with *Eco*RV or *Ahd*I (1 h, 37ºC). After analysis on denaturing PAGE, cleavage by SSEs + *Eco*RV should release a 1740 nt 5′-Cy5-labelled fragment. Cleavage by SSEs + *Ahd*I should release a 129 nt 5′-Cy5-labelled fragment. (**E**) D3 D-loops processing by Mus81 and Yen1 after digestion with *Eco*RV. The red arrowhead indicates the 1716 bp fragment (Cy5 labelled) and black arrowhead indicates the 1242 bp fragment (unlabelled). Cleavage products were separated through an agarose gel that was first scanned for Cy5 with a Typhoon FLA9500 (left), and then post-stained with EtBr and imaged with a GelDoc (right). The dashed line indicates gel cropping and removing of irrelevant lanes. Labels: N, Nicked; L, Linear; SC, Supercoiled. (**F**) Reaction products of D3 D-loops processing by Mus81 and Yen1, followed by DNA ligation and cleavage with *Eco*RV were analysed on a 10% denaturing PAGE. The dual-coloured arrows indicate the invading strand ligated to the plasmid backbone. Expected products are depicted on the right. Labels: Y, Yen1; M, Mus81; EV, *EcoRV*. (**G**) Same as (F) but using *Ahd*I restriction enzyme for product analysis. Labels: Y, Yen1; M, Mus81; EV, *EcoRV*; AI, *Ahd*I.

consistent with the formation of a more open structure containing two nicks, where the invading strand remains paired with pBSK and displays a 3′-ssDNA flap resulting from the Yen1 incision at the end of the displaced strand (Figure 7D). Based on our mapping, we predicted that this incision would position the 3′-end of the invading strand in close proximity to the newly generated 5′-phosphate end, enabling theoretical ligation and transfer of the 5′-Cy5 label to the plasmid. To test this hypothesis, we performed subsequent cleavage with *Eco*RV (Figure 7D), which should generate two linear molecules of approximately 1.2 and 1.7 kb, with the latter being Cy5-labelled (Figure 7D). Indeed, when we subjected the reaction products from treatment of D3 D-loops with Mus81 and Yen1 to *Eco*RV digestion, we observed the disappearance of the Cy5-labelled band with slower migration and the appearance of a new band of similar intensity of around 1.7 kb (Figure 7E, left panel, red arrowhead). Ethidium bromide staining of the same gels further revealed the presence of an unlabelled 1.2 kb band (Figure 7E, right panel, black arrowhead). Importantly, the generation of these products required the combined activity of Yen1, Mus81, and *Eco*RV, but did not require the presence of T4 ligase (Figure 7E, compare lanes 5 and 6 in both panels). To ascertain if the invading strand was indeed ligated to the plasmid, we repeated the experiments and analysed the samples using denaturing PAGE, which should reveal the presence of high molecular weight bands only if the ligation occurred (Figure 7D and F; 3058 nt expected size: 2958 nt from pBSK plus 100 nt from D2 oligo). Indeed, the presence of Cy5-labelled DNA was observed in the wells of the gels only when Yen1, Mus81, and T4 ligase were present (Figure 7F). Further digestion with *Eco*RV enabled the entry of the DNA into the gel, despite its short migration difference (Figure 7F, compare lanes 5 and 6). To further confirm the production of the expected molecule, we performed the experiments with *Ahd*I digestion, which cleaves closer to the ligation point and thus released a smaller, 129 nt-long Cy5-labelled DNA fragment, which migrates faster in the gel (Figure 7G, compare lanes 8 and 9). These results provide compelling evidence for the ligation of the invading DNA strand to the recipient plasmid, resulting in the formation of a nicked molecule that represents a direct precursor of a half-crossover.

Discussion

Genetic data from several groups have implicated Mus81 and Yen1 structure-selective endonucleases (SSEs) in the processing of repair intermediates involved in or leading to BIR (26,70–72). Interestingly, it has also been suggested that the processing of early recombination intermediates, such as D-loops, by Mus81 and Yen1 could result in the formation of aberrant repair outcomes, including chromosomal loss and half-crossover events, implying a need for a thorough regulation of the SSEs activities (28,35,37,70). Using a biochemical approach, we provide mechanistic insight supporting these observations by comprehensively characterizing the activity of Mus81 and Yen1 on various D-loop structures.

To mimic different stages of D-loop formation, we examined a nascent D-loop (D3), an extended D-loop (D2), and a D-loop with no overhangs (D1), which are widely used models for analysis of *in vitro* D-loop processing. Generally, the cleavage sites detected for Mus81 on the synthetic D3 D-loop (Figure 1) are in agreement with the previous reports (43–45), as well as the absence of activity on the D2 D-loop (43). For the D1 D-loop, the incisions happen on the opposite strand (the displaced strand) compared to the D3 D-loop (Figure 1 and Supplementary Figure S2), reflecting similarity to a 3′-flap-like structure cleaved by Mus81 (44). For Yen1, we demonstrate for the first time its ability to process all three types of D-loops. We identified an invariant cleavage site on the distal end of the displaced strand in all D-loop structures and observed Yen1's ability to incise the invading strands (Figure 1). The locations of these cleavage sites are consistent with the expected 5′ polarity of a Rad2/XPG-family nuclease.

Importantly, the main incision sites remain unchanged when similar D-loop structures are enzymatically reconstituted in a plasmid-based assay (Figures 3, 6, and Supplementary Figure S7-S9). Nevertheless, D-loop deproteinization prior to nuclease action facilitates the cleavage of both Yen1 and Mus81 (Supplementary Figure S6), suggesting that Rad51, Rad54, and RPA may influence substrate accessibility to the nucleases, although they do not significantly alter the position of the incisions. Indeed, the stabilization of the Rad51 filament in the presence of the non-hydrolysable ATP analogue ATPγS (73) (Figure 5) severely reduced cleavage by Mus81 and Yen1, respectively. These experiments point to a possibility that the ATP binding mode of Rad51 and its regulation by Rad51 mediator proteins (e.g. Rad51 paralogs), may play a role in the regulation of Mus81 and Yen1 processing. Additionally, Rad51 has been previously shown to represent a barrier to the catalytic activity of Mus81 (51). In fact, the same study has also shown that Mus81 interacts with Srs2, enabling Mus81 to access its substrate by removing Rad51 from DNA through the 'strippase' activity of Srs2 and stimulating directly the Mus81 catalytic activity (51). While not formally tested here, the potential effect of Rad54 in modulating SSE activity on D-loops by steric hindrance can also be readily envisaged, due its known presence at D-loop branchpoints (74–77). Thus, it would be intriguing to explore this possibility in further investigations.

In line with this, RECQ5, a functional human homolog of Srs2, has been found to be required for the removal of RAD51 from late replication intermediates at common fragile sites to facilitate their processing by MUS81-EME1 (78). Similarly, FBH1, another potential human homolog of Srs2, has been shown to cooperate with MUS81 following replication stress (79). The Srs2 strippase activity is also crucial to prevent the formation of toxic joint molecules during BIR, where long stretches of ssDNA accumulate and may be bound by Rad51, leading to promiscuous invasion events (28). Importantly, this work indicates that the expression of Yen1^{ON} (a Yen1 mutant insensitive to cell cycle-dependent control (66,80)) increases HC and CL events, but only in the presence of Srs2 (28), suggesting that D-loop-bound Rad51 could prevent their processing by Yen1. These findings collectively highlight the essential role of Rad51 and its accessory proteins in processing of joint molecules and the prevention of undesirable recombination outcomes.

Finally, our study provides biochemical evidence supporting the genetic observations indicating that concurrent actions of Mus81 and Yen1 on D-loop structures may facilitate chromosomal rearrangements that occur in the context of BIR, like HCs (28,36,37). The specific locations of the incisions generated by Mus81 on the non-displaced strand and Yen1 on the displaced strand of the donor DNA are compatible with the generation of HC products if the invading molecule is ligated to the donor through the nicks created by these SSEs (Figure 8

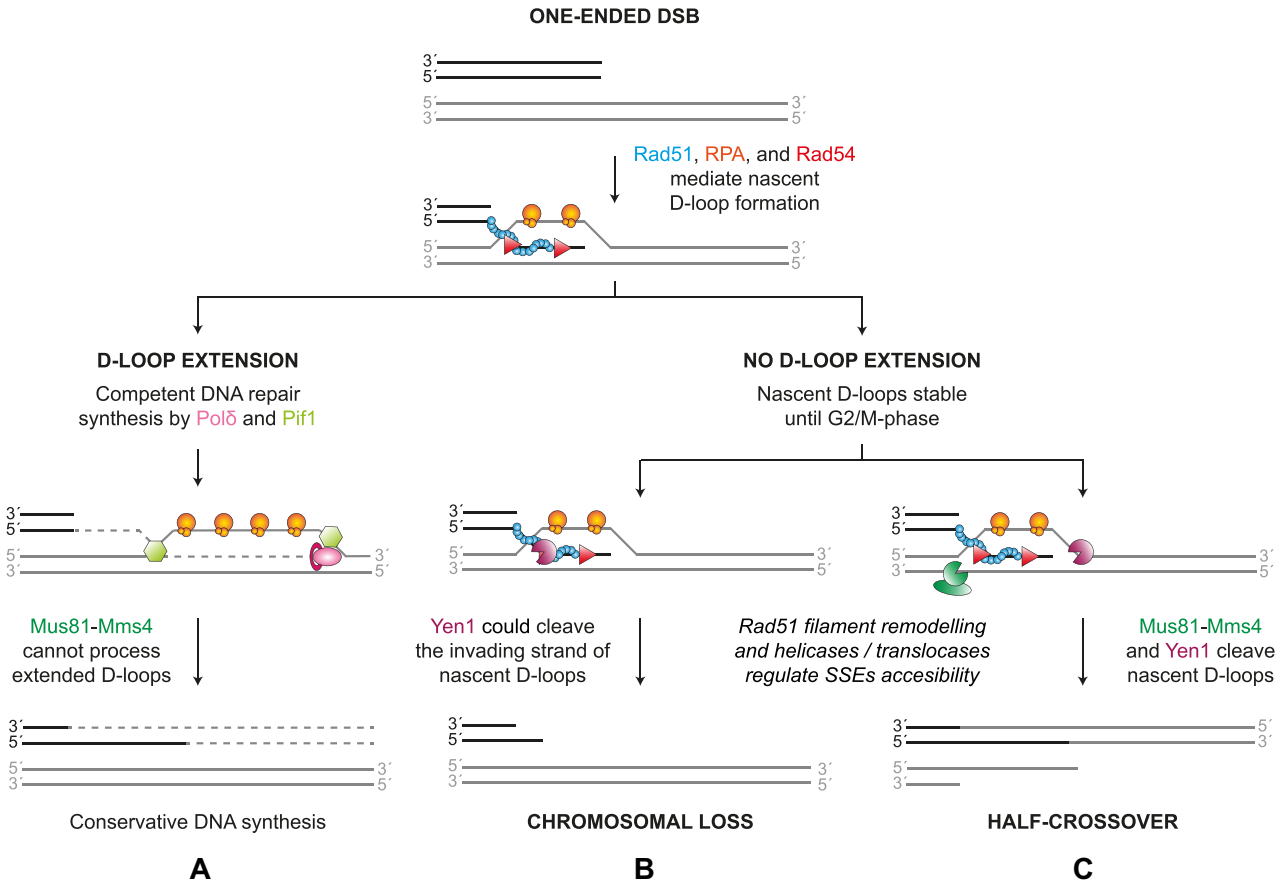

Figure 8. Model for the generation of chromosomal loss and half-crossover events due to Mus81-Mms4 and Yen1 activity on BIR intermediates. Protein names and cartoons are colour coded. (**A**) After nascent D-loops are formed, *de novo* DNA synthesis and bubble migration render the D-loops insensitive to Mus81-Mms4 action, allowing their extension until they reach a convergent replication fork or the end of the chromosome. (**B**) Persistent nascent D-loop structures that are not extended may become substrates for the SSEs later in the cell cycle or upon premature SSE activation, leading to nascent D-loop cleavage. In this scenario, Yen1 nicking activity at the invading strand may result in a chromosomal loss event. SSE accessibility to this substrate might be regulated by Rad51 filament remodelling, by Rad51 paralogs or any other factor that affects Rad51 ATP hydrolysis. (**C**) As in (B) but depicting the combined actions of Mus81-Mms4 and Yen1 leading to a half-crossover event. In addition to Rad51 filament remodelling, several helicases/translocases that have been proposed to modulate Mus81-Mms4 activity could influence the frequency of this outcome (e.g. Rad54, Srs2, see Discussion section).

and Supplementary Figure S3A). Indeed, we demonstrate that the addition of a ligase in our reconstituted D-loop reactions, following Mus81 and Yen1 treatment, allows ligation of the invading strand to the donor molecule (Figure 7). However, since Mus81 incisions occur 4–5 nt from the first branching point (Supplementary Figure S7), the resulting small ssDNA gap would prevent ligation. Congruently, we were unable to detect the second ligation event between the short strand of the invading molecule and the pBSK donor (data not shown). Furthermore, we noticed that when Mus81 and Yen1 were incorporated simultaneously, Yen1 was no longer able to cleave the invading strand (Figure 7F). This is most likely due to the Mus81 incision allowing rotation of the D-loop into a RF-like structure where the invasion point is no longer a branched structure that can be targeted by Yen1. Since the cleavage of the invading strand by Yen1 most likely leads to CL events (Figure 8 and Supplementary Figure S3B), it would be interesting to address in the future whether the absence of Mus81 increases CL events in a BIR system described by Elango *et al.* upon Yen1^{ON} expression.

Additionally, using synthetic substrates, we determined that the Yen1 incisions at the equivalent D3 D-loop structure were independent, with the cleavage on the displaced strand occurring much faster than the cleavage on the invading oligo (Figure 2). HCs are proposed to arise after D-loop formation during BIR if DNA synthesis is compromised due to defects in Polδ (36–38) or Pif1 (24,26,64,81), both of which are required for extensive DNA synthesis. Failure to initiate DNA synthesis in these mutants could lead to the resolution of a single HJ generated after strand invasion, and Mus81 has been suggested to play a role in the generation of these genetic products (37). In addition, there is a long delay between strand invasion and the beginning of DNA synthesis within the D-loop (82), which might be due to the activation of a recombination execution checkpoint in the absence of a second end at the DSB (83,84). In this context, it is plausible that the nascent D-loops formed in S or early G2 phases may not be extended until later stages of the cell cycle, when Mus81 and Yen1 become activated (85). If DNA synthesis within the D-loops begins, the migration of the bubble would separate the invasion point from the complementary strand of the invading molecule (24), leading to a structure similar to the D2 D-loop. In this configuration, Mus81 would no longer be able to cleave, allowing error-prone BIR synthesis to proceed (Figures 1, 3, and 8). Therefore, we favour the possibility that any potential cleavage by Mus81 on an extended D-loop would more

likely occur after the synthesis of the lagging strand near the invasion point, creating a structure more similar to the D3 D-loop. Moreover, it has been demonstrated that premature SSE activation and entry to mitosis, due to a compromised checkpoint response in cells undergoing BIR, also stimulates HC formation (38).

It is important to acknowledge certain technical limitations in our study, albeit they do not alter its main conclusions. First, in some of our experiments involving oligonucleotide-based D-loops, appearance of minor bands was observed. These bands cannot be solely attributed to the incisions made by the SSEs, suggesting the possibility of partial disassembly of nicked synthetic D-loops during the reactions or their electrophoretic separation (Figure 1 and Supplementary Figure S2). Second, the comparison of gels scanned for fluorescent oligonucleotides with EtBr staining (i.e. Supplementary Figure S6B), alongside control reactions conducted in the absence of the invading oligo and/or Rad51/Rad54, respectively, show that, especially for Yen1, a small fraction of the nicked circles (about 10%) detected in the EtBr-stained gels stems from direct nicking of the donor plasmid, independently of D-loop formation. This is likely a consequence of the alkaline lysis method used for donor plasmid preparation, as it may lead to trace amounts of partially denatured plasmid allowing annealing of invading oligo even in the absence of recombinases, and thus becoming a substrate for the SSEs. Therefore, this should be considered with respect to the quantitative aspects of donor plasmid processing by the SSEs.

Our findings provide a biochemical framework for the genetic observations implicating Mus81 and Yen1 in the generation of the chromosomal loss and half-crossover events, but it is important to highlight that in our system, we have used the minimal protein ensemble required for D-loop formation *in vitro*. Therefore, it cannot be ruled out that other proteins involved in their generation or stabilization *in vivo* may modulate D-loop processing by these nucleases. In the future, it would be therefore interesting to optimize a system that allows us to measure SSE activity after D-loop extension and/or bubble migration, which could be promoted by the addition of RFC/PCNA/Polδ and/or Pif1. Such a system would also allow us to demonstrate if the sensitivity of D-loops to the action of nucleases varies at different stages of their maturation. Altogether, we consider that this type of studies enhance our understanding of the complex interplay between DNA repair pathways that prevent genome instability and pathological chromosomal aberrations.

Data availability

The data underlying this article are available in the article and in its online Supplementary material.

Supplementary data

Supplementary Data are available at NAR Online.

Acknowledgements

We wish to thank members of the Krejci and Blanco laboratories for useful discussions.

Author contributions. Raquel Carreira: Conceptualization, Data curation, Formal analysis, Investigation, Methodology, Validation, Visualization, Writing—original draft, Writing—review & editing. Tomas Lama-Diaz, Maria Crugeiras, and F. Javier Aguado: Investigation, Writing—review & editing. Marek Sebesta: Resources, Writing—review & editing. Lumir Krejci: Conceptualization, Funding acquisition, Methodology, Resources, Supervision, Writing—review & editing. Miguel G. Blanco: Conceptualization, Funding acquisition, Methodology, Project administration, Resources, Supervision, Writing—original draft, Writing—review & editing.

Funding

The work in the Blanco lab was supported by Ministerio de Ciencia e Innovación y Agencia Estatal de Investigación/10.13039/501100011033 [PID2020-115472GB-I00]; Ministerio de Ciencia e Innovación, Agencia Estatal de Investigación and Fondo Europeo de Desarrollo Regional 'Una manera de hacer Europa' [BFU2016-78121-P]; Xunta de Galicia and Fondo Europeo de Desarrollo Regional 'Una manera de hacer Europa' [ED431F- 2016/019, ED431B-2016/016 and ED431C 2019/013]; the work in the Krejci lab was supported by the Czech Science Foundation [21-22593X]; Wellcome Trust collaborative grant [206292/E/17/Z]; R.C., T.L.D., M.C. and F.J.A. were supported by pre-doctoral fellowships from Xunta de Galicia [ED481A-2018/041, ED481A-2018/042, ED481A-2015/011, ED481A 2022/155]; M.C. was also supported by a Collaboration fellowship from 'Asociación Española Contra el Cáncer'; CIMUS receives financial support from the Xunta de Galicia and Fondo Europeo de Desarrollo Regional [ED431G 2019/02, Centro Singular de Investigación de Galicia, accreditation 2019–2022]. Funding for open access charge: Ministerio de Ciencia e Innovación y Agencia Estatal de Investigación/10.13039/501100011033 [PID2020-115472GB-I00].

Conflict of interest statement

None declared.

References

1. Moynahan,M.E. and Jasin,M. (2010) Mitotic homologous recombination maintains genomic stability and suppresses tumorigenesis. *Nat. Rev. Mol. Cell Biol.*, **11**, 196–207.
2. Symington,L.S., Rothstein,R. and Lisby,M. (2014) Mechanisms and regulation of mitotic recombination in saccharomyces cerevisiae. *Genetics*, **198**, 795–835.
3. Cejka,P. and Symington,L.S. (2021) DNA end resection: mechanism and control. *Annu. Rev. Genet.*, **55**, 285–307.
4. Krejci,L., Altmannova,V., Spirek,M. and Zhao,X. (2012) Homologous recombination and its regulation. *Nucleic Acids Res.*, **40**, 5795–5818.
5. Heyer,W.D. (2015) Regulation of recombination and genomic maintenance. *Cold Spring Harb. Perspect. Biol.*, **7**, a016501.
6. Kowalczykowski,S.C. (2015) An overview of the molecular mechanisms of recombinational DNA repair. *Cold Spring Harb. Perspect. Biol.*, **7**, a016410.
7. Mehta,A. and Haber,J.E. (2014) Sources of DNA double-strand breaks and models of recombinational DNA repair. *Cold Spring Harb. Perspect. Biol.*, **6**, a016428.
8. Van Komen,S., Petukhova,G., Sigurdsson,S., Stratton,S. and Sung,P. (2000) Superhelicity-driven homologous DNA pairing by yeast recombination factors Rad51 and Rad54. *Mol. Cell*, **6**, 563–572.
9. Wright,W.D. and Heyer,W.D. (2014) Rad54 Functions as a heteroduplex DNA pump modulated by its DNA substrates and Rad51 during D loop formation. *Mol. Cell*, **53**, 420–432.

10. Petukhova,G., Van Komen,S., Vergano,S., Klein,H. and Sung,P. (1999) Yeast Rad54 promotes Rad51-dependent homologous DNA pairing via ATP hydrolysis-driven change in DNA double helix conformation. *J. Biol. Chem.*, **274**, 29453–29462.
11. Crickard,J.B., Moevus,C.J., Kwon,Y., Sung,P. and Greene,E.C. (2020) Rad54 Drives ATP hydrolysis-dependent DNA sequence alignment during homologous recombination. *Cell*, **181**, 1380–1394.
12. Li,X. and Heyer,W.D. (2009) RAD54 controls access to the invading 3′-OH end after RAD51-mediated DNA strand invasion in homologous recombination in Saccharomyces cerevisiae. *Nucleic Acids Res.*, **37**, 638–646.
13. Fasching,C.L., Cejka,P., Kowalczykowski,S.C. and Heyer,W.D. (2015) Top3-Rmi1 dissolve Rad51-mediated D loops by a topoisomerase-based mechanism. *Mol. Cell*, **57**, 595–606.
14. Liu,J., Ede,C., Wright,W.D., Gore,S.K., Jenkins,S.S., Freudenthal,B.D., Washington,M.T., Veaute,X. and Heyer,W.D. (2017) Srs2 promotes synthesis-dependent strand annealing by disrupting DNA polymerase d-extending D-loops. *eLife*, **6**, e22195.
15. Ira,G., Malkova,A., Liberi,G., Foiani,M. and Haber,J.E. (2003) Srs2 and Sgs1-Top3 suppress crossovers during double-strand break repair in yeast. *Cell*, **115**, 401–411.
16. Prakash,R., Satory,D., Dray,E., Papusha,A., Scheller,J., Kramer,W., Krejci,L., Klein,H., Haber,J.E., Sung,P., *et al.* (2009) Yeast Mphl helicase dissociates Rad51-made D-loops: implications for crossover control in mitotic recombination. *Genes Dev.*, **23**, 67–79.
17. Sebesta,M., Burkovics,P., Haracska,L. and Krejci,L. (2011) Reconstitution of DNA repair synthesis in vitro and the role of polymerase and helicase activities. *DNA Repair (Amst.)*, **10**, 567–576.
18. Bzymek,M., Thayer,N.H., Oh,S.D., Kleckner,N. and Hunter,N. (2010) Double Holliday junctions are intermediates of DNA break repair. *Nature*, **464**, 937–941.
19. Wu,L. and Hickson,I.O. (2003) The Bloom's syndrome helicase suppresses crossing over during homologous recombination. *Nature*, **426**, 870–874.
20. Bizard,A.H. and Hickson,I.D. (2014) The dissolution of double Holliday junctions. *Cold Spring Harb. Perspect. Biol.*, **6**, a016477.
21. Wyatt,H.D.M. and West,S.C. (2014) Holliday junction resolvases. *Cold Spring Harb. Perspect. Biol.*, **6**, a023192.
22. Schwartz,E.K. and Heyer,W.D. (2011) Processing of joint molecule intermediates by structure-selective endonucleases during homologous recombination in eukaryotes. *Chromosoma*, **120**, 109–127.
23. Liu,L. and Malkova,A. (2022) Break-induced replication: unraveling each step. *Trends Genet.*, **38**, 752–765.
24. Saini,N., Ramakrishnan,S., Elango,R., Ayyar,S., Zhang,Y., Deem,A., Ira,G., Haber,J.E., Lobachev,K.S. and Malkova,A. (2013) Migrating bubble during break-induced replication drives conservative DNA synthesis. *Nature*, **502**, 389–392.
25. Donnianni,R.A. and Symington,L.S. (2013) Break-induced replication occurs by conservative DNA synthesis. *Proc. Natl. Acad. Sci. U.S.A.*, **110**, 13475–13480.
26. Wilson,M.A., Kwon,Y., Xu,Y., Chung,W.H., Chi,P., Niu,H., Mayle,R., Chen,X., Malkova,A., Sung,P., *et al.* (2013) Pif1 helicase and polδ promote recombination-coupled DNA synthesis via bubble migration. *Nature*, **502**, 393–396.
27. Mayle,R., Campbell,I.M., Beck,C.R., Yu,Y., Wilson,M., Shaw,C.A., Bjergbaek,L., Lupski,J.R. and Ira,G. (2015) Mus81 and converging forks limit the mutagenicity of replication fork breakage. *Science*, **349**, 742–747.
28. Elango,R., Sheng,Z., Jackson,J., Decata,J., Ibrahim,Y., Pham,N.T., Liang,D.H., Sakofsky,C.J., Vindigni,A., Lobachev,K.S., *et al.* (2017) Break-induced replication promotes formation of lethal joint molecules dissolved by Srs2. *Nat. Commun.*, **8**, 1790.
29. Sakofsky,C.J., Roberts,S.A., Malc,E., Mieczkowski,P.A., Resnick,M.A., Gordenin,D.A. and Malkova,A. (2014) Break-induced replication is a source of mutation clusters underlying kataegis. *Cell Rep.*, **7**, 1640–1648.
30. Ruff,P., Donnianni,R.A., Glancy,E., Oh,J. and Symington,L.S. (2016) RPA stabilization of single-stranded DNA is critical for break-induced replication. *Cell Rep.*, **17**, 3359–3368.
31. Bosco,G. and Haber,J.E. (1998) Chromosome break-induced DNA replication leads to nonreciprocal translocations and telomere capture. *Genetics*, **150**, 1037–1047.
32. Malkova,A. (2018) Break-induced replication: the where, the why, and the How. *Trends Genet.*, **34**, 518–531.
33. Anand,R.P., Tsaponina,O., Greenwell,P.W., Lee,C.S., Du,W., Petes,T.D. and Haber,J.E. (2014) Chromosome rearrangements via template switching between diverged repeated sequences. *Genes Dev.*, **28**, 2394–2406.
34. Ruiz,J.F., Gómez-González,B. and Aguilera,A. (2009) Chromosomal translocations caused by either Pol32-dependent or Pol32-independent triparental break-induced replication. *Mol. Cell. Biol.*, **29**, 5441–5454.
35. Pardo,B. and Aguilera,A. (2012) Complex chromosomal rearrangements mediated by break-induced replication involve structure-selective endonucleases. *PLoS Genet.*, **8**, e1002979.
36. Deem,A., Barker,K., VanHulle,K., Downing,B., Vayl,A. and Malkova,A. (2008) Defective break-induced replication leads to half-crossovers in Saccharomyces cerevisiae. *Genetics*, **179**, 1845–1860.
37. Smith,C.E., Lam,A.F. and Symington,L.S. (2009) Aberrant double-strand break repair resulting in half crossovers in mutants defective for Rad51 or the DNA polymerase complex. *Mol. Cell. Biol.*, **29**, 1432–1441.
38. Vasan,S., Deem,A., Ramakrishnan,S., Argueso,J.L. and Malkova,A. (2014) Cascades of genetic instability resulting from compromised break-induced replication. *PLoS Genet.*, **10**, e1004119.
39. Piazza,A., Wright,W.D. and Heyer,W.D. (2017) Multi-invasions are recombination byproducts that induce chromosomal rearrangements. *Cell*, **170**, 760–773.
40. Piazza,A. and Heyer,W.D. (2019) Homologous recombination and the formation of complex genomic rearrangements. *Trends Cell Biol.*, **29**, 135–149.
41. Savocco,J. and Piazza,A. (2021) Recombination-mediated genome rearrangements. *Curr. Opin. Genet. Dev.*, **71**, 63–71.
42. Reitz,D., Djeghmoum,Y., Watson,R.A., Rajput,P. and Argueso,J.L. (2023) Delineation of two multi-invasion-induced rearrangement pathways that differently affect genome stability. *Genes Dev.*, **37**, 621–639.
43. Osman,F., Dixon,J., Doe,C.L. and Whitby,M.C. (2003) Generating crossovers by resolution of nicked Holliday junctions: a role for Mus81-Eme1 in meiosis. *Mol. Cell*, **12**, 761–774.
44. Ehmsen,K.T. and Heyer,W.D. (2009) A junction branch point adjacent to a DNA backbone nick directs substrate cleavage by saccharomyces cerevisiae Mus81-Mms4. *Nucleic Acids Res.*, **37**, 2026–2036.
45. Pepe,A. and West,S.C. (2014) Substrate specificity of the MUS81-EME2 structure selective endonuclease. *Nucleic Acids Res.*, **42**, 3833–3845.
46. Ehmsen,K.T. and Heyer,W.D. (2008) Saccharomyces cerevisiae Mus81-Mms4 is a catalytic, DNA structure-selective endonuclease. *Nucleic Acids Res.*, **36**, 2182–2195.
47. Ehmsen,K.T. and Heyer,W.D. (2009) A junction branch point adjacent to a DNA backbone nick directs substrate cleavage by saccharomyces cerevisiae Mus81-Mms4. *Nucleic Acids Res.*, **37**, 2026–2036.
48. Mukherjee,S., Wright,W.D., Ehmsen,K.T. and Heyer,W.D. (2014) The Mus81-Mms4 structure-selective endonuclease requires nicked DNA junctions to undergo conformational changes and bend its DNA substrates for cleavage. *Nucleic Acids Res.*, **42**, 6511–6522.
49. Schwartz,E.K., Wright,W.D., Ehmsen,K.T., Evans,J.E., Stahlberg,H. and Heyer,W.-D. (2012) Mus81-Mms4 Functions as a single

heterodimer to cleave nicked intermediates in recombinational DNA repair. *Mol. Cell. Biol.*, **32**, 3065–3080.
50. Matulova,P., Marini,V., Burgess,R.C., Sisakova,A., Kwon,Y., Rothstein,R., Sung,P. and Krejci,L. (2009) Cooperativity of Mus81·Mms4 with Rad54 in the resolution of recombination and replication intermediates. *J. Biol. Chem.*, **284**, 7733–7745.
51. Chavdarova,M., Marini,V., Sisakova,A., Sedlackova,H., Vigasova,D., Brill,S.J., Lisby,M. and Krejci,L. (2015) Srs2 promotes Mus81-Mms4-mediated resolution of recombination intermediates. *Nucleic Acids Res.*, **43**, 3626–3642.
52. Benitez,A., Sebald,M., Kanagaraj,R., Rodrigo-brenni,M.C., Chan,Y.W., Liang,C., West,S.C., Benitez,A., Sebald,M., Kanagaraj,R., *et al.* (2023) GEN1 promotes common fragile site expression. *Cell Rep.*, **42**, 112062.
53. Carreira,R., Aguado,F.J., Lama-Diaz,T. and Blanco,M.G. (2021) Holliday junction resolution. *Methods Mol. Biol.*, **2153**, 169–185.
54. Princz,L.N., Wild,P., Bittmann,J., Aguado,F.J., Blanco,M.G., Matos,J. and Pfander,B. (2017) Dbf4-dependent kinase and the Rtt107 scaffold promote Mus81-Mms4 resolvase activation during mitosis. *EMBO J.*, **36**, 664–678.
55. Van Komen,S., Macris,M., Sehorn,M.G. and Sung,P. (2006) Purification and assays of saccharomyces cerevisiae homologous recombination proteins. *Methods Enzymol.*, **408**, 445–463.
56. Petukhova,G., Sung,P. and Klein,H. (2000) Promotion of Rad51-dependent D-loop formation by yeast recombination factor Rdh54/Tid1. *Genes Dev.*, **14**, 2206–2215.
57. Gupta,R.K., Gupta,P., Yushok,W.D. and Rose,Z.B. (1983) Measurement of the dissociation constant of MgATP at physiological nucleotide levels by a combination of 31P NMR and optical absorbance spectroscopy. *Biochem. Biophys. Res. Commun.*, **117**, 210–216.
58. Sherman,F. (2002) Getting started with yeast. *Methods Enzymol.*, **350**, 3–41.
59. Janke,C., Magiera,M.M., Rathfelder,N., Taxis,C., Reber,S., Maekawa,H., Moreno-Borchart,A., Doenges,G., Schwob,E., Schiebel,E., *et al.* (2004) A versatile toolbox for PCR-based tagging of yeast genes: new fluorescent proteins, more markers and promoter substitution cassettes. *Yeast*, **21**, 947–962.
60. Houseley,J. and Tollervey,D. (2011) Repeat expansion in the budding yeast ribosomal DNA can occur independently of the canonical homologous recombination machinery. *Nucleic Acids Res.*, **39**, 8778–8791.
61. Chee,M.K. and Haase,S.B. (2012) New and redesigned pRS plasmid shuttle vectors for genetic manipulation of saccharomyces cerevisiae. *G3: Genes Genomes Genetics*, **2**, 515–526.
62. Blanco,M.G., Matos,J., Rass,U., Ip,S.C.Y. and West,S.C. (2010) Functional overlap between the structure-specific nucleases Yen1 and Mus81-Mms4 for DNA-damage repair in S. cerevisiae. *DNA Repair (Amst.)*, **9**, 394–402.
63. Pepe,A. and West,S.C. (2014) MUS81-EME2 promotes replication fork restart. *Cell Rep.*, **7**, 1048–1055.
64. Buzovetsky,O., Kwon,Y., Pham,N.T., Kim,C., Ira,G., Sung,P. and Xiong,Y. (2017) Role of the Pif1-PCNA complex in pol δ-dependent strand displacement DNA synthesis and break-induced replication. *Cell Rep.*, **21**, 1707–1714.
65. Killelea,T., Saint-Pierre,C., Ralec,C., Gasparutto,D. and Henneke,G. (2014) Anomalous electrophoretic migration of short oligodeoxynucleotides labelled with 5′-terminal Cy5 dyes. *Electrophoresis*, **35**, 1938–1946.
66. Carreira,R., Aguado,F.J., Hurtado-Nieves,V. and Blanco,M.G. (2022) Canonical and novel non-canonical activities of the Holliday junction resolvase Yen1. *Nucleic Acids Res.*, **50**, 259–280.
67. Eggler,A.L., Inman,R.B. and Cox,M.M. (2002) The Rad51-dependent pairing of long DNA substrates is stabilized by replication protein A. *J. Biol. Chem.*, **277**, 39280–39288.
68. Van Komen,S., Petukhova,G., Sigurdsson,S. and Sung,P. (2002) Functional cross-talk among Rad51, Rad54, and replication protein A in heteroduplex DNA joint formation. *J. Biol. Chem.*, **277**, 43578–43587.
69. Li,X., Zhang,X.P., Solinger,J.A., Kiianitsa,K., Yu,X., Egelman,E.H. and Heyer,W.D. (2007) Rad51 and Rad54 ATPase activities are both required to modulate Rad51-dsDNA filament dynamics. *Nucleic Acids Res.*, **35**, 4124–4140.
70. Ho,C.K., Mazón,G., Lam,A.F. and Symington,L.S. (2010) Mus81 and Yen1 promote reciprocal exchange during mitotic recombination to maintain genome integrity in budding yeast. *Mol. Cell*, **40**, 988–1000.
71. Pardo,B., Moriel-Carretero,M., Vicat,T., Aguilera,A. and Pasero,P. (2020) Homologous recombination and Mus81 promote replication completion in response to replication fork blockage. *EMBO Rep.*, **21**, e49367.
72. Bittmann,J., Grigaitis,R., Galanti,L., Amarell,S., Wilfling,F., Matos,J. and Pfander,B. (2020) An advanced cell cycle tag toolbox reveals principles underlying temporal control of structure-selective nucleases. *eLife*, **9**, e52459.
73. Zaitseva,E.M., Zaitsev,E.N. and Kowalczykowski,S.C. (1999) The DNA binding properties of saccharomyces cerevisiae Rad51 protein. *J. Biol. Chem.*, **274**, 2907–2915.
74. Wright,W.D. and Heyer,W.D. (2014) Rad54 Functions as a heteroduplex DNA pump modulated by its DNA substrates and Rad51 during D loop formation. *Mol. Cell*, **53**, 420–432.
75. Tavares,E.M., Wright,W.D., Heyer,W.D., Le Cam,E. and Dupaigne,P. (2019) In vitro role of Rad54 in Rad51-ssDNA filament-dependent homology search and synaptic complexes formation. *Nat. Commun.*, **10**, 4058.
76. Li,X. and Heyer,W.D. (2009) RAD54 controls access to the invading 3′-OH end after RAD51-mediated DNA strand invasion in homologous recombination in *Saccharomyces cerevisiae*. *Nucleic Acids Res.*, **37**, 638–646.
77. Kiianitsa,K., Solinger,J.A., Heyer,W.-D. and Kolodner,R.D. (2006) Terminal association of Rad54 protein with the Rad51-dsDNA filament. *Proc Natl Acad Sci U S A*, **103**, 9767–9772.
78. Di Marco,S., Hasanova,Z., Kanagaraj,R., Chappidi,N., Altmannova,V., Menon,S., Sedlackova,H., Langhoff,J., Surendranath,K., Hühn,D., *et al.* (2017) RECQ5 Helicase cooperates with MUS81 endonuclease in processing stalled replication forks at common fragile sites during mitosis. *Mol. Cell*, **66**, 658–671.
79. Fugger,K., Chu,W.K., Haahr,P., Nedergaard Kousholt,A., Beck,H., Payne,M.J., Hanada,K., Hickson,I.D. and Sørensen,C.S. (2013) FBH1 co-operates with MUS81 in inducing DNA double-strand breaks and cell death following replication stress. *Nat. Commun.*, **4**, 1423.
80. Blanco,M.G., Matos,J. and West,S.C. (2014) Dual control of Yen1 nuclease activity and cellular localization by cdk and Cdc14 prevents genome instability. *Mol. Cell*, **54**, 94–106.
81. Sakofsky,C.J., Ayyar,S., Deem,A.K., Chung,W.H., Ira,G. and Malkova,A. (2015) Translesion polymerases drive microhomology-mediated break-induced replication leading to complex chromosomal rearrangements. *Mol. Cell*, **60**, 860–872.
82. Malkova,A., Naylor,M.L., Yamaguchi,M., Ira,G. and Haber,J.E. (2005) RAD51 -Dependent break-induced replication differs in kinetics and checkpoint responses from RAD51 -mediated gene conversion. *Mol. Cell. Biol.*, **25**, 933–944.
83. Jain,S., Sugawara,N., Lydeard,J., Vaze,M., Gac,N.T.L. and Haber,J.E. (2009) A recombination execution checkpoint regulates the choice of homologous recombination pathway during DNA double-strand break repair. *Genes Dev.*, **23**, 291–303.
84. Jain,S., Sugawara,N., Mehta,A., Ryu,T. and Haber,J.E. (2016) Sgs1 and Mph1 helicases enforce the recombination execution checkpoint during DNA double-strand break repair in saccharomyces cerevisiae. *Genetics*, **203**, 667–675.
85. Blanco,M.G. and Matos,J. (2015) Hold your horSSEs: controlling structure-selective endonucleases MUS81 and Yen1/GEN1. *Front. Genet.*, **6**, 253.

Received: September 22, 2023. **Revised:** May 5, 2024. **Editorial Decision:** May 11, 2024. **Accepted:** May 14, 2024